Journal Pre-proofs

Formulation optimization of ritonavir tablets containing spray dried dispersion from HPMCAS-L or PVP-VA and comparative dissolution/permeation performance

Ayse Nur Oktay, James E. Polli

PII: S0378-5173(25)01048-8
DOI: https://doi.org/10.1016/j.ijpharm.2025.126211
Reference: IJP 126211

To appear in: *International Journal of Pharmaceutics*

Received Date: 20 July 2025
Revised Date: 10 September 2025
Accepted Date: 23 September 2025

Please cite this article as: A.N. Oktay, J.E. Polli, Formulation optimization of ritonavir tablets containing spray dried dispersion from HPMCAS-L or PVP-VA and comparative dissolution/permeation performance, *International Journal of Pharmaceutics* (2025), doi: https://doi.org/10.1016/j.ijpharm.2025.126211

Formulation Optimization of Ritonavir Tablets Containing Spray Dried Dispersion from HPMCAS-L or PVP-VA and Comparative Dissolution/Permeation Performance

Ayse Nur Oktay[a,b,*], James E. Polli[a]

[a] University of Maryland, Department of Pharmaceutical Sciences, Baltimore, MD 21201, USA

[b] University of Health Sciences, Gulhane Faculty of Pharmacy, Department of Pharmaceutical Technology, Ankara, Turkey

*Corresponding author. e-mail address: aysenur.oktay@sbu.edu.tr

ABSTRACT

Tablets are the most preferred oral dosage form due to advantages such as high-speed manufacturing, cost-effectiveness, stability, and patient compliance. Amorphous solid dispersions (ASDs) can enhance the solubility and bioavailability of poorly soluble drugs, but a strategic approach to convert ASD powders into tablets is lacking. This study aimed to optimize formulation and process for tablets containing ritonavir-HPMCAS-L ASD powders and compare its dissolution/permeation performance to tablets employing PVP-VA. Microcrystalline cellulose(MCC) and dibasic calcium phosphate(DCP) were evaluated as fillers, while croscarmellose sodium(CCS), crospovidone(CP) and sodium starch glycolate(SSG) served as disintegrants. Optimization considered two SDD powder levels, two disintegrant levels, and two spray-drying inlet temperatures (70 and 140°C). Further process optimization tested various compaction forces via direct compression and dry granulation. Tablet optimization of ritonavir using HPMCAS-L identified the following optimum parameters, including favorable in vitro dissolution: dry granulation (14kN pre- compression +7kN compression), 65.5% SDD intermediate, 10% CCS as a disintegrant, 24% MCC as a filler and 0.5% magnesium stearate as lubricant. Applying these parameters to ritonavir ASD tablets fabricated with PVP-VA, SoluPlus, HPMCAS-L and HPMCAS-L:H resulted in HPMCAS-L also exhibiting favorable in vitro dissolution, like PVPV-VA. When subjected to dissolution/permeation evaluation, tablets with PVP-VA exhibited higher ritonavir permeation than those from HPMCAS-L. Tablets with PVP-VA showed ritonavir permeation like from Norvir tablets, and solution from Norvir powder. These results may reflect the dissolution-resulting colloid as a critical component to overall drug absorption from ASD, beyond even favorable dissolution.

Keywords: Ritonavir, Spray Dryer, Tablet, Optimization, Dissolution, Permeation, Absorption

1. INTRODUCTION

Tablets are the most preferred oral dosage form since have the advantages of high-speed manufacturing, lower cost of goods, higher stability, convenience of dosing, ease of handling, self-administration and better patient compliance (Arshad et al., 2021). Tablets are also the common dosage form of amorphous solid dispersions (ASD), although ASD powders have low flowability. There are numerous marketed ASD tablets (e.g. Sporanox, Norvir, Intelence, Kaletra , Zelboraf and Incivek) and ASD tablets in clinical trials (Bhujbal et al., 2021; Chakravarty et al., 2017; Moseson et al., 2024).

Although viewed as a last resort formulation approach due to costs and development risk, ASDs have demonstrated to ability to enhance the solubility and bioavailability of

poorly-soluble drugs. Relative to the crystalline state, the amorphous state can provide high solubility and greater dissolution since no energy is required to break the drug crystal lattice (Bhujbal et al., 2021; Vaka et al., 2014). ASDs can be prepared by spray drying which is commercially scalable and a continuous process (Ogawa et al., 2018; Singh and Van den Mooter, 2016). An ASD prepared by spray drying is denoted to be a spray dried dispersion (SDD). Spray drying is a complex unit operation with parameters which affect resulting SDD powder properties and thus tabletability. However, there are a limited number of studies concerning the overall approach to transform an SDD powder into a tablet dosage form, even though SDD powder can exhibit poor flow and needs rapid dispersion to provide the desired higher dissolution.

To modulate powder properties and render SDD powder potentially suitable for tablet formulation, excipients selection entails the identification of filler, disintegrant and lubricant for tableting for potential direct compression or dry granulation. Diluents increase the tablet bulk and potentially address ASD-related issues of inadequate flowability, poor compaction properties, and capping. Disintegrants promote drug surface area exposure and thus facilitate dissolution (Aguiar et al., 1968; Démuth et al., 2015). Commonly used diluents are starch, lactose, microcrystalline cellulose (MCC), dibasic calcium phosphate (DCP), sucrose and mannitol; and commonly used disintegrants are sodium starch glycocholate (SSG), croscarmellose sodium (CCS), and crospovidone (CP) (DiNunzio et al., 2012; Honick et al., 2020a; Yu and Hoag, 2024). Excipient type and amounts can impact stability, hardness and dissolution profiles of tablets (Démuth et al., 2015; Fakes et al., 2009; Faroongsarng and Peck, 1994).

Moreover, the tableting method can affect the performance of the tablets containing ASD. ASDs are subjected to mechanical stress during compression and dry granulation, which may impact their physical stability. In wet granulation processes, exposure to solvents can induce both crystallization and phase separation between distinct amorphous components (Ayenew et al., 2012; Duddu and Sokoloski, 1995; Hancock and Zografi, 1994). Iyer et al. investigated the effects of ASD manufacturing methods (spray drying and melt extrusion) on tablet compaction properties (e.g. compression pressure, elastic modulus, tensile strength, dynamic hardness) (Iyer et al., 2013). Honick et al. evaluated the effects of the grade of the hydroxypropyl methylcellulose acetate succinate (HPMCAS) polymer, compaction speed and spray drying process on the tablets containing itraconazole ASD powders (Honick et al., 2020a). Yu et al. highlighted the impact of diluents on the compaction, dissolution performance and stability of the tablets containing itraconazole and HPMCAS ASD (Yu and Hoag, 2024).

In this study, ritonavir (RTN) was selected as a model drug. There are several marketed drug products containing RTN. For example, Norvir tablets contain an ASD of RTN, where the ASD was prepared via hot melt extrusion (HME). Paxlovid (nirmatrelvir tablets /ritonavir tablets) is used to treat COVID-19 infection, where RTN boosts the pharmacokinetic of nirmatrelvir by inhibiting nirmatrelvir metabolism via CYP3A inhibition; RTN tablets are a component of Paxlovid and also contain an ASD of RTN. Given the potential need for additional anti-COVID-19 drugs and additional drugs that may benefit from ritonavir boosting their pharmacokinetics (e.g. lopinavir, such as Kaletra), ritonavir was selected as a model lowly soluble drug. RTN's low aqueous solubility (1 µg/ml) limits its oral bioavailability, such that all marketed tablets of RTN employ RTN as an ASD. Furthermore, in fabricating RTN as an ASD

intermediate, all marketed tablets of RTN employ polyvinylpyrrolidone-vinyl acetate (PVP-VA) (i.e. copovidone) as the ASD polymer (Moseson et al., 2024). PVP-VA is an excipient with decades of prior use, including prior to the development of Norvir tablets in the 1990's.

A more recently introduced polymer for ASD fabrication is HPMCAS, including the L-grade (i.e. HPMCAS-L) with a higher content of succinoyl function group than other HPMCAS grades. In our earlier work, we performed computational assessments of drug–polymer interactions combined with preliminary experimental evaluations to screen six polymers alongside PVP-VA, for their suitability in formulating amorphous solid dispersions of ritonavir (Oktay and Polli, 2024). Findings indicated that HPMCAS-L was most preferable, along with, as expected, PVP-VA. Cast films of RTN and HPMCAS-L showed favorable dissolution compared to amorphous ritonavir without polymer, including at even a high drug load of 40%. Of course, cast films are not representative of a final dose form such as a tablet, or representative of an underpinning ASD unit operation such as spray drying. Hence, while these film casting findings are optimistic for pairing RTN with a new dissolution-enabling polymer, a gap is the successful development of a viable tablet containing an RTN/HPMCAS-L ASD (e.g. powder flowability, sufficient compaction properties, no capping, adequate dissolution), particularly given the limited number of studies concerning the overall approach to transform an ASD powder into a tablet dosage form.

In this study, an aim was to optimize formulation and process for tablets containing ritonavir-HPMCAS-L ASD powders and compare its dissolution/permeation performance to tablets employing PVP-VA. A series of formulation development studies were subsequently carried out and are presented herein. The process began with the optimization of formulation components using microcrystalline cellulose (MCC) and dibasic calcium phosphate (DCP) as fillers, along with sodium starch glycolate (SSG), croscarmellose sodium (CCS), and crospovidone (CP) as disintegrants. Process parameters were optimized using a Styl'One compaction simulator under varying compaction force conditions. Tablet properties were also compared following direct compaction and dry granulation. After the optimization of process and formulation parameters for RTN-HPMCAS-L tablet, the same parameters were applied with HPMCAS L:H, SoluPlus and PVP-VA polymers to assess the effects of polymer types on the tablet properties. Dissolution and permeation studies were performed on the optimum tablet with these polymers, and their comparative dissolution/permeation performances were evaluated.

2. MATERIALS AND METHODS

2.1 Materials

RTN was obtained from ChemShuttle (Blue Current Inc., Hayward, CA). Aquasolve HPMCAS-L and HPMCAS-H were provided by Ashland (Ashland Inc; Covington, KY). PVP-VA (Kollidon®VA 64) and SoluPlus were provided by BASF (Ludwigshafen Germany). Solvents dichloromethane and methanol to prepare the SDD powders were analytical grade and purchased from Sigma Aldrich (St. Louis, MO) and Fischer

Scientific (Hampton, NH). Fillers microcrystalline cellulose (MCC) and dibasic calcium phosphate (DCP) were obtained from JRS Pharma (Patterson, NY). Sodium starch glycocholate (SSG), croscarmellose sodium (CCS), and crospovidone (CP) were used as disintegrants and gifted from JRS Pharma (Patterson, NY). The lubricant magnesium stearate was obtained from Roquette (Lower Gwynedd Township, PA).

A hollow fiber membrane (HFM) module was purchased from Repligen (Repligen Corp; Marlborough, MA). The HFM module contained a surface area of 115 cm^2 (area/volume: 0.128/cm as media volume was 900mL) via 36 small hollow fiber membranes (i.e., parallel tubes, composed of PES). The membrane had a pore size of 300 KDa (MWCO). Dimensions of membrane fibers were 0.5 mm ID, 0.2 mm thickness, and 20 cm length.

2.2 Overall approach

Overall, studies here involved a tablet formulation phase and a subsequent in vitro dissolution/permeation evaluation phase. Firstly, **Figure 1** illustrates the tablet formulation phase, which entailed four sequenced studies, denoted study 1, study 2, study 3, and study 4. Studies 1-3 focused on developing a tablet formulation containing the SDD of RTN and HPMCAS-L. The impact of composition and process parameters on tablet properties were evaluated, where each study's conclusions were employed in the subsequent study. Study 1 and study 2 focused on optimizing tablet formulation parameters. In study 1, tablet formulation parameters were optimized using a 2^3 (3 repeated) full factorial design, where SDD powder level and disintegrant level were varied, along with inlet temperature during spray drying to fabricate SDD. In study 2, tablet formulation parameters were further optimized, where filler type and disintegrant type were evaluated. Study 1 and 2 used direct compression, as direct compression is less robust than dry granulation, in order to arrive at a formulation composition that could be potentially viable even for direct compression. For each direct compression and dry granulation, Study 3 employed optimum formulation composition to assess compression force influence, using a Styl'One compaction simulator. In each study, several tablet and/or tableting attributes were characterized, including in vitro dissolution. The result from study 3 was an optimized RTN tablet using SDD from HPMCAS-L, where tableting process and formulation parameters using HPMCAS-L were optimized.

Study 4 applied these optimized process and formulation parameters to the fabrication of RTN tablets that used SDD from each PVP-VA, SoluPlus, and HPMCAS-L:H (1:1 w/w ratio) polymers. In compaction of tablets using SDD of each PVP-VA, SoluPlus, and HPMCAS-L:H, tablet hardness was kept constant, to match that of tablets from optimized HPMCAS-L tablets. In performing in vitro dissolution studies, the commercial Norvir tablet formulation, where the SDD intermediate from hot melt extrusion contains RTN and PVP-VA, was also tested, as a comparator. As USP apparatus II vessel dissolution results show (e.g. yielding k_d), RTN tablets from HPMCAS-L and PVP-VA performed best and were subjected to subsequent in vitro dissolution/permeation evaluation.

Secondly, **Figure 2** illustrates the subsequent in vitro dissolution/permeation evaluation phase, with the goal to predict the intestinal permeation of RTN from the optimum HPMCAS-L and PVP-VA tablet formulations, as well as Norvir tablets. Dissolution/permeation studies used the D-HFM system. Briefly, RTN permeation rate

coefficient (i.e. k_p) from a solution of RTN, obtained by dissolving Norvir powder, was measured across a HFM module. Then, the permeation of RTN from each the optimum HPMCAS-L tablet formulation, the optimum PVP-VA tablet formulation, and Norvir tablet was predicted, using the k_p from the RTN solution and k_d from the RTN tablet. Predicted D-HFM absorption profiles were compared to observed D-HFM absorption profiles.

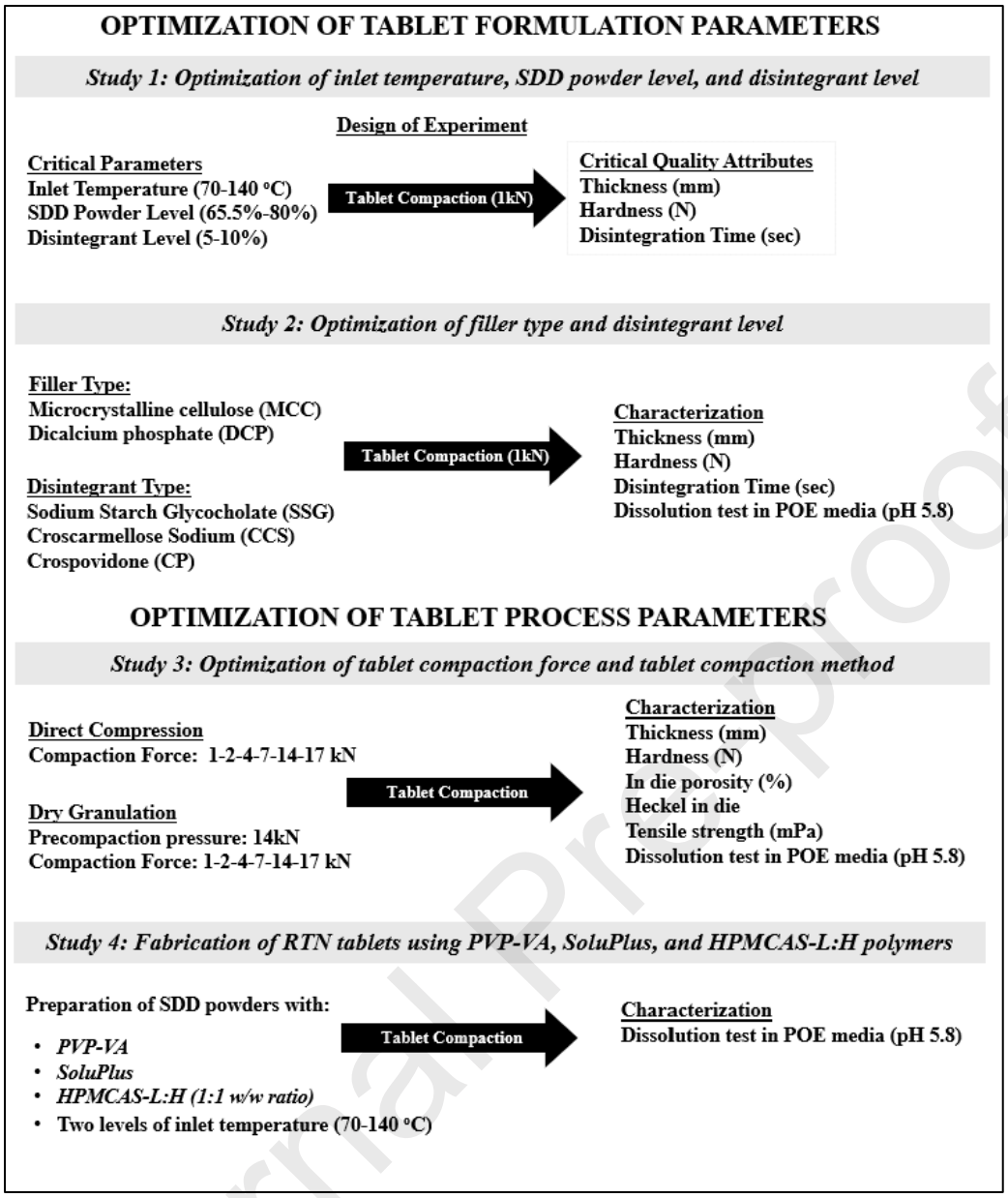

Figure 1. Scope and sequence of tablet formulation studies. Study 1 and study 2 focused on optimizing tablet formulation parameters, using HPMCAS-L. Study 3 focused on tablet process parameters, using HPMCAS-L. As results show, study 1 informed the use of lower SDD powder level (i.e. 65.5%), higher disintegrant level (i.e. 10%), and lower spray drier inlet temperature (i.e. 70°C) for subsequent study 2. Study 2 informed the use of MCC as filler and CCS as disintegrant in subsequent study 3. Study 3 identified the preference for dry granulation, including 14+7 kN compaction force. Study 4 applied these optimized process and formulation parameters to the fabrication of RTN tablets that used SDD from each PVP-VA, SoluPlus, and HPMCAS-L:H (1:1 w/w ratio). RTN tablets from HPMCAS-L and PVP-VA performed best and were subjected to subsequent in vitro dissolution/permeation evaluation.

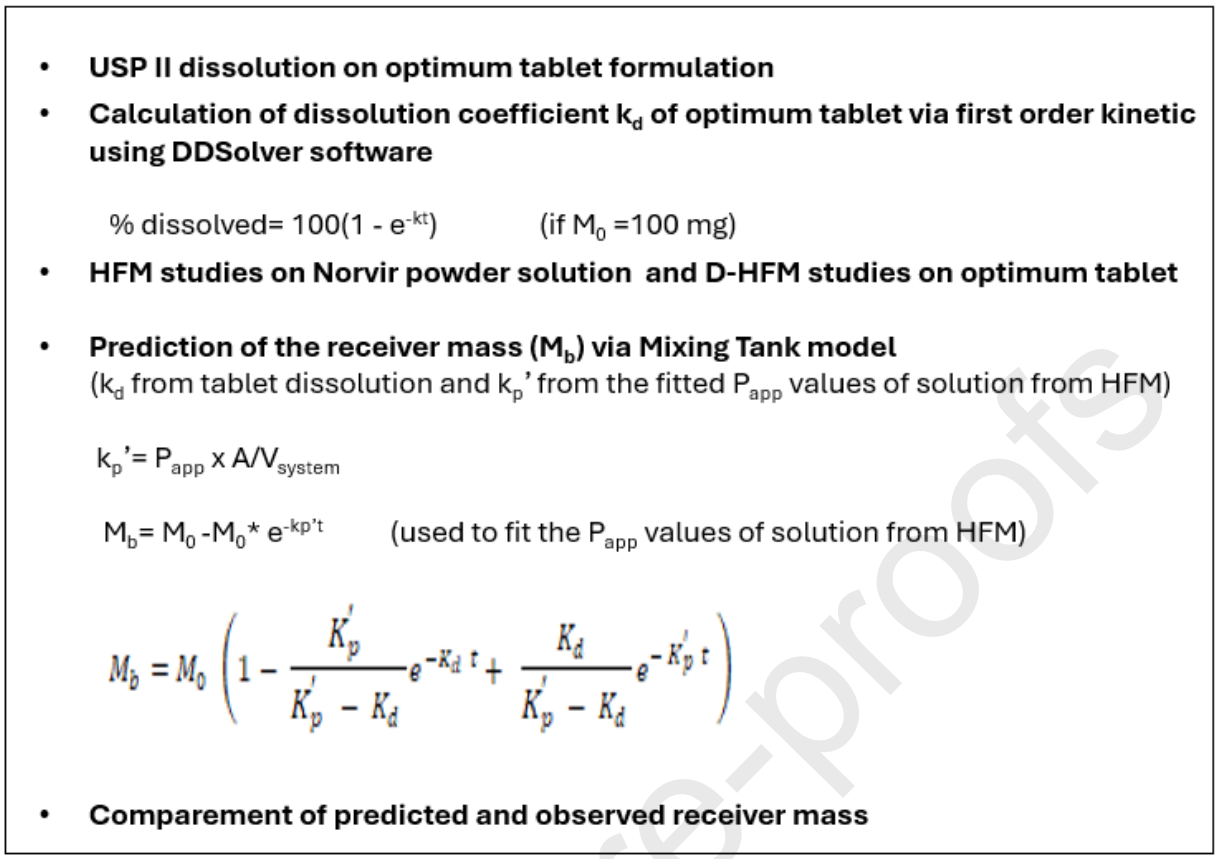

Figure 2. Scope and sequence of in vitro dissolution/permeation studies, after study 4 of tablet formulation studies. Dissolution/permeation studies used the D-HFM system. Also listed are USP II dissolution studies from the prior tablet formulation phase of studies, resulting in dissolution rate coefficient k_d. Tested formulations were tablet formulations that employed SDD from each HPMCAS-L and PVP-VA, along with commercial Norvir tablet. HFM permeation rate coefficient k_p was estimated from subjecting a solution fabricated from commercial Norvir powder to HFM permeation. For each of the two test tablets and Norvir tablets, predicted D-HFM absorption profiles were constructed from k_d and k_p, then compared to observed D-HFM absorption profiles.

2.3 RTN spray dried dispersion

Tablets were prepared containing 100mg of RTN, where the drug was in the form of an SDD from spray drying. Spray-dried powders of RTN were prepared by using a Buchi B-290 spray dryer (BUCHI Corporation; New Castle, DE) in closed-loop mode. Solid content (RTN and HPMCAS-L) was 10% w/v and RTN:HPMCAS-L ratio was 20:80 w/w (i.e. 20% drug loading into SDD powder). Solutions were prepared in 2:1 of dichloromethane:methanol (Oktay and Polli, 2024). Firstly, HPMCAS-L was solved in organic solvent and then the RTN was added into the polymer solution. From preliminary studies, the RTN-polymer solution was mixed using a magnetic stirrer. The homogenous solutions were pumped into the spray dryer using a spray gas flow rate of 742 L/h (i.e. 60 mm height of pump setting), solution feed rate of 6 mL/min (i.e. 20% of setting) and an aspirator rate of 38 m^3/h (i.e. 100% setting). Two inlet temperatures in study 1 were examined, 70°C and 140 °C, to assess the effect of the inlet temperature on tablet compression. The SDDs were collected and dried for an

additional 12 h at 40°C and stored in a desiccating cabinet (RH < 5%) (Honick et al., 2020b).

Separately, SDD powders were also prepared with HPMCAS L:H, SoluPlus and PVP-VA polymers to assess the effects polymer types. They used the same method as described above for HPMCAS-L, including the same solvent system.

2.4 SDD characterization

True densities, thermal analysis and scanning electron microscopy (SEM) analysis were performed on RTN SDD powder samples (of each HPLCAS-L, HPMCAS L:H, SoluPlus and PVP-VA) to examine the effect tablet porosity and inlet temperature on tablet tabletability. True density refers to the intrinsic density of individual particles, excluding any interstitial spaces or voids. In contrast, bulk density represents the average mass-to-volume ratio of a powder sample, typically measured in the presence of air or another surrounding medium. A helium pycnometer (AccuPyc 1330, MicroMeritics, Norcross, US) was used to determine true density (n=3) (Yu and Hoag, 2024). Helium pycnometer parameters were: 10 runs, 10 purges and 19.5 psig as purge and run fill pressure.

For thermal analysis, approximately 5–10 mg of each sample (RTN powder, HPMCAS-L, HPMCAS L:H, SoluPLus, PVP-VA polymers, or SDD powder of each) were sealed in Tzero pans and analyzed on a Discovery DSC 2500 (TA Instruments) with a 50 mL min^{-1} nitrogen purge. A heat/cool/reheat cycle (to 200 °C → 30 °C → 200 °C; 10 °C min^{-1} throughout) was applied. T_g values for polymers and RTV SDDs were obtained from the second heating trace in TRIOS (Oktay and Polli, 2024). From thermal analysis, crystalline RTN showed a melting endotherm at 128.2 °C, while all SDDs were amorphous, with no RTN melting endotherm at 128.2°C.

For scanning electron microscopy (SEM), the samples were affixed to specimen stubs using conductive carbon adhesive tabs (Ted Pella, Redding, CA). A thin layer of platinum/palladium alloy (approximately 10–20 nm) was applied via sputter coating using an EMS 150T ES system (Electron Microscopy Sciences, Hatfield, PA). SEM micrographs were captured with a Quanta 200 instrument (FEI Co., Hillsboro, OR) under the imaging parameters noted in the corresponding figure legends (Honick et al., 2020b). True densities and scanning electron microscopy (SEM) analysis were also performed on RTN coarse powder and physical mixture of RTN and polymers, as comparators to SDD powder.

2.5 Optimization of tablet formulation and process parameters: Overall approach

Tablet formulation studies involved studies 1-4 (Figure 1). Four studies involved tableting to fabricate tablets containing 100 mg of RTN from SDD intermediate with 20% drugs load (i.e. 80% polymer load in SDD). In all studies, tablets were prepared using a STYL'One Evolution compaction simulator (Medelpharm; Lyon, France). Tooling was 11.28 mm flat faced round tooling (99.93 mm^2). All studies used 0.5% magnesium stearate (MgS) as the lubricant. After weighing drug and all excipients, all powders except the lubricant were poured into a glass jar according to the geometric dilution method and mixed using a Turbula Shaker Mixer Type T2F (Glen Mills Inc.; Clifton, NJ) for 5 min. Then, lubricant was added, and the jar was mixed for 1 min.

In all studies, 100mg RTN tablets weighed 763.64mg (for 65.5% of SDD powder level) and 625 mg (for 80% of SDD powder level) and were compressed with 0.4000x0.75 inch capsule type tooling. The lower punch was set to a fill depth of 23.5 mm, yielding a total fill volume of 2.35 mL. To ensure consistent punch velocity (approximately 1 mm/s), a symmetrical sawtooth waveform was applied to both the upper and lower punches throughout compression.

2.5.1 Optimization of tablet formulation parameters: study 1 and study 2

Study 1 examined SDD powder level and disintegrant level, along with spray drying inlet temperature. Examination of SDD powder level (i.e. 65.5% versus 80%, of entire tablet weight) was motivated by the need to allow for only 20% drug loading into SDD powder intermediate, to obtain ASD benefits, such as enhanced dissolution without rapid precipitation (Adhikari and Polli, 2020). In particular, previously, film formulations of RTN were prepared with various polymers using 20% and 40% drug load (Oktay and Polli, 2024). A RTN crystalline peak was not observed in 20% films but observed in 40% films, indicating RTN crystallization at 40%. Moreover, during the solubilization capacity studies, RTN release was higher for 20% than for 40% with HPMCAS-L, PVP-VA and SoluPlus polymers. So, 20% drug load was selected here.

Examination of disintegrant level (i.e. 5% versus 10%) was motivated by the need for rapid disintegration, particularly since HPMCAS is known to gel if not quickly dispersed, and since RTN is poorly soluble. A third factor was spray drying inlet temperature (i.e. 70^{o}C versus 140^{o}C). While this factor is a spray drying process factor, inlet temperature (and hence SDD formation and drying) can impact resulting SDD powder (e.g. size) and tableting properties, as results show.

To carry out study 1, a 2^3 full factorial design (3 repeated) was designed using StatEase DoE software (Version 12) (Stat-Ease, Inc.; Minneapolis, MN). Table S1 shows the design, with each factor studied at two levels**.** Direct compression was performed using 1 kN for tablet compression. Tablets were characterized in terms of thickness, hardness, and disintegration time, per USP disintegration. As results show, study 1 informed the use of lower SDD powder level (i.e. 65.5%), higher disintegrant level (i.e. 10%), and lower spray drier inlet temperature (i.e. 70^{o}C) for subsequent study 2.

Study 2 examined filler type (i.e. MCC versus DCP) and disintegrant type (SSG versus CCS versus CP). Study 1 only used MCC as filler and SSG as disintegrant. Favorably, MCC allowed the lower filler level for successful tablets in study 1. Less favorably, SSG required higher disintegrant level for successful tablets in study 1. Hence, two alternatives to SSG were evaluated in study 2. Table S2 lists the compositions of the six evaluated tablets. Tablets employed SDD that was fabricated using 70^{o}C inlet air temperature. Direct compression was performed using 1 kN for tablet compression. Tablets were characterized in terms of thickness, length, width, hardness, disintegration time, and dissolution. Dissolution was carried out per a modified USP monograph method for ritonavir tablets, where maleic acid was used in place of phosphate buffer. Study 2 informed the use of MCC as filler and CCS as disintegrant in subsequent study 3.

2.5.2 Optimization of tablet process parameters: study 3

Study 3 focused on tablet process parameters (Figure 1). As shown below, study 1 and 2 collectively resulted in the following tablet composition being used in study 3: 65.5% SDD powder, 24% MCC as filler, 10% CCS as disintegrant, and 0.5% MgS as lubricant. Both direct compression and dry granulation were conducted, using a STYL'One Evolution compaction simulator with a target weight of 763.64mg (and 100mg RTN). Direct compression was performed using various compaction forces (i.e. 1, 2, 4, 7, 14, or 17 kN). Dry granulation was conducted using a 14kN pre-compression force. Resulting compacts were triturated using a mortar and pestle to produce granules, which were then sieved using a 30-mesh sieve. Granules, which passed though the 30-mesh sieve, were compressed using various compaction forces (i.e. 1, 2, 4, 7, 14, or 17 kN). Adjustments were applied to account for the elastic deformation of the punches (i.e. 0.00565 mm/kN), using a correction factor. Compaction profiles were recorded and processed using the AnalisMX software (version 2.07.9; Medelpharm, Lyon, France). Tablet hardness, thickness, mean compaction force (kN), mean compaction pressure (mPa), in die porosity (%), Heckel in die (Ln(1/(1-D))), and tensile strength (mPa) were determined, per below. USP II dissolution (i.e. paddle method) was conducted using maleic acid buffer with 60mM POE (pH 5.8) at 37 °C.

2.5.3 Tablet alternatives to HPMCAS-L: HPMCAS L:H, SoluPlus and PVP-VA: study 4

RTN tablets using SDD powder intermediates of each HPMCAS L:H, SoluPlus and PVP-VA were fabricated using the same formulation and process conditions (except 4kN tablet compaction force for PVP-VA and SoluPlus tablets) that were optimal from using HPMCAS-L. Their SDD powder intermediates were obtained as described above.

2.6 Characterization of tablet physical properties

Tablet length (mm), width (mm) and thickness (mm) were measured (n=3) using a digital caliper (WALTER; Anif, Austria). Tablet hardness was measured using a MultiTest 50 hardness tester (Pharmatron; Solothurn, Switzerland).

In assessing the effects of compaction force in study 3, mean compaction force (i.e. yield force applied during the tablet compaction) was recorded from the STYL'One software (n=3). Compaction pressure was calculated via Eq. 4:

$$\text{Compaction pressure(mPa)} = \text{Compaction force(N)}/\text{Area (mm}^2\text{)} \qquad \text{Eq.4}$$

Area (i.e. tablet die hole surface area) was 171.39 mm^2.

Tensile strength (σ_t; MPa) was calculated by using Eq.5:

$$\sigma_t = \frac{2P}{\pi dt} \qquad \text{Eq.5}$$

where *P* denotes the tablet breaking force (in Newtons), *d* represents the tablet diameter (in millimeters), and *t* corresponds to the out-of-die thickness (in millimeters).

Powder compressibility profiles were analyzed using the in-die porosities. Tablet percent porosity (ε) was calculated via Eq.6:

$$\varepsilon = \left[1 - \frac{w}{v\rho_t}\right]x100 \quad \text{Eq.6}$$

where w is the compact weight, v is compact volume, and ρ_t is compact true density.

Commonly used in the analysis of powder compression, the Heckel equation (Eq. 7) is an empirical equation based on the linear portion of the compression pressure (P) versus relative density (D) curve:

$$\ln\left(1 - \frac{1}{1-D}\right) = KP + A \quad \text{Eq.7}$$

here *K* denotes the slope of the linear region and *A* represents the y-intercept of the Heckel plot (Yu et al., 2024). The reciprocal of *K* represents the yield pressure (Py), indicating the pressure threshold at which the material transitions to plastic deformation. Heckel analysis was conducted using the AnalisMX software package (v2.07.9).

2.7 Tablet disintegration

The in vitro disintegration time was estimated using digital disintegration test apparatus with single drum according to USP method (United States Pharmacopeia). Distilled water at 37.0 ± 0.5 °C was used as the test fluid (Iwao et al., 2013). A tablet was placed in each of six tubes and then a disc was added. Disintegration was taken to be completed when the tablet showed no palatableness mass remaining.

2.8 Tablet dissolution using USP II apparatus

Tablets were subjected to USP II dissolution testing using a USP II apparatus (SR8PLUS, Hanson Research; Chatsworth CA). Dissolution was carried out per a modified USP monograph method for ritonavir tablets, where maleic acid was used in place of phosphate buffer. A single dissolution medium using 50 mM maleic acid buffer with 60mM polyoxyethylene 10 lauryl ether (POE) (pH 5.8) was purposely applied across all formulations. USP II dissolution testing on each formulations (n=3) employed 900 ml of 50 mM maleic acid buffer with 60mM polyoxyethylene 10 lauryl ether (POE) (pH 5.8) at 37°C at 75 rpm. At predetermined time intervals (0, 5, 10, 20, 30, 45, 60, 90, 120, 180, 240, and 360 minutes), 2 mL aliquots were withdrawn from the sample. Each aliquot was subsequently filtered using a 0.45 µm Millipore membrane filter. At each sampling, 2 ml of fresh dissolution media was added to each vessel. Drug was quantified using HPLC as described below.

In study 4, the dissolution studies were also performed on the RTN tablets prepared with HPMCAS L:H, SoluPlus and PVP-VA polymers. The hardness levels of tablets were kept constant for all polymers to see the effects of polymers on dissolution profiles, without an impact from hardness. Tablet dissolution profiles from USP II dissolution testing were fitted to the first-order dissolution profile, yielding k_d for each tablet formulation (Polli et al., 1997). Non-linear regression was performed using Excel Solver to estimate k_d (Polli, 2022). Dissolution data analysis included area under the

dissolution curve (AUC) assessment, in optimum formulation and process parameters examination. Moreover, f_2 calculation was conducted to compare the in vitro dissolution profiles of SDD tablets to Norvir tablet (Seo et al., 2002).

Dissolving ASD can form colloids via Liquid-Liquid Phase Separation (LLPS) (Dhumal et al., 2024; Indulkar et al., 2019; Men and Polli, 2024). Dynamic Light Scattering (DLS) was used to measure colloid size of PVP-VA and HPMCAS-L SDD powders that were subjected to in vitro dissolution in 50 mM maleic acid buffer (pH 5.8) with 60mM POE10, as well as 50 mM maleic acid buffer (pH 5.8) without surfactant. 2mL sample was taken at 0, 5,15, 30, 60, 120, 180, and 360 minutes. Colloid size in dissolution samples was determined using a Malvern Zetasizer Nano ZSP. A 1 mL sample was centrifuged for 5 minutes at 13,400 rpm to pellet any undissolved drug (Stewart et al., 2017). Measurements were taken using a 12 mm square polystyrene disposable cuvette with 173° backscattered light, after the samples had equilibrated at 37°C for 120 seconds (Nunes et al., 2023; Yang et al., 2021).

2.9 Permeation of RTN Through Hollow Fiber Membrane (HFM) Module

As result show, test tablets fabricated using HPMCAS-L and PVP-VA were selected for dissolution/permeation evaluation. Prior to performing D-HFM studies of the two test tablets and Norvir tablets and observing in vitro RTN absorption, it was desirable to predict RTN in vitro absorption. Here, in vitro absorption denotes drug dissolution and permeation from in vitro D-HFM testing, and not only drug dissolution (e.g. from USP II vessel testing) nor only drug permeation (e.g. from HFM testing of drug solution).
Hence, RTN permeation across a HFM module from an apparent solution (0.111 mg/mL) was conducted, as previously described (Adhikari et al., 2022a, b). RTN solution was prepared by dissolving Norvir® powder (100 mg) in the dissolution media, prior to addition of the dissolution media to the system. Of note, Norvir® powder contains amorphous RTN in the form of an ASD fabricated with PVP-VA via hot melt extrusion (HME) (Pandi et al., 2020). Dissolution media was 900 mL of maleic acid buffer with 60 mM POE 10 (pH 5.8). HFM receiver solution was also maleic acid buffer with 60 mM POE 10 (pH 5.8). The donor and receiver flow rates were 2ml/min using a peristaltic pump (Cole Parmer, IL). As described above for tablet dissolution studies, two ml of sample was obtained at 0, 5, 10, 20, 30, 45, 60, 90, 120, 180, 240 and 360 min from receiver and donor compartments. Samples were through a 0.45 mm Millipore filter. The permeation coefficient (P_{app}), flux (J_s), and the permeated amount of RTN were calculated (Adhikari et al., 2022a, b).

k'_p was calculated using eq 8:

$$k'_p = \left(\frac{A}{V}\right) x\ P_{app} \qquad \text{Eq. 8}$$

where P_{app} is the observed HFM permeability from the solution study, and $\frac{A}{V}$ is the ratio of area of HFM membrane to donor volume (i.e. 115 cm^2 /900 ml or 0.128/cm).

2.10 Predicted RTN in vitro absorption from optimized tablets

Per Figure 2, RTN in vitro absorption from each optimized tablet formulation, as well as Norvir tablets, was predicted using the previously described Mixing Tank model

(Adhikari et al., 2022a). Experimentally, two inputs were k_d from USP II vessel dissolution studies (above), along with k'_p from the solution HFM study (above). Predicted RTN in vitro absorption profile was estimates from:

$$M_b = M_0\left(1 - \frac{k'_p}{k'_p - k_d}e^{-k_d t} + \frac{k_d}{k'_p - k_d}e^{-k'_p t}\right) \quad \text{Eq. 9}$$

where M_b is the cumulative mass absorbed by D-HFM system, and M_0 is the initial drug mass in the donor (i.e. 100mg).

Of note, the ratio of M_b versus M_0 is percent drug permeation into receiver.

2.11 D-HFM from optimized tablets, observed RTN in vitro absorption, and comparison to predicted in vitro absorption

Dissolution-permeation system using D-HFM has been previously characterized as a potential permeation component of a dissolution/permeation system to assess oral drug absorption (Adhikari et al., 2022a, b). Using combined USP II vessel and HFM, D-HFM studies were conducted on the optimum RTN tablet formulations with HPMCAS-L, HPMCAS L:H, SoluPlus and PVP-VA polymers, as well as commercial Norvir tablet. The set up was identical to that described above for HFM of RTN solution, except optimized tablets (and not dissolved Norvir powder) were tested, and paddle was present and rotated at 75 rpm.

Observed receiver mass profiles (M_b versus time) were compared to predicted profiles. Additionally, observed flux (J_s) was calculated (Adhikari et al., 2022a). Also, observed P_{app} and k'_p were calculated using eq 9, using k_d from USP II vessel dissolution studies. Tablet dissolution profiles from USP II vessel dissolution studies and from D-HFM studies were comparable.

2.12 Quantification of ritonavir by HPLC

For all dissolution, permeation, and dissolution/permeation studies, HPLC was used to determine RTN concentration using a Waters 2489 HPLC system (Waters Corporation; Milford, MA), with a UV-vis detector. An isocratic mobile phase consisting of 47% acetonitrile and 53% phosphoric acid (0.05M) solution was used, with a 25.0 µL injection volume and a flow rate of 1 mL/min. A 4.6 × 150-mm Zorbax C18 5-µm HPLC column was used (Karakucuk et al., 2016). The UV-vis detector was set to 240 nm (Karakucuk et al., 2016; Karakucuk et al., 2019). The retention time of RTN was 9-10 min, with a 13 min run time. A calibration curve containing 50 µg/mL, 25 µg/mL, 12.5 µg/mL, 6.25 µg/mL, 3.125 µg/mL, 1.56 µg/mL, 0.78 µg/mL, 0.39 µg/mL, 0.195 µg/mL, 0.098 µg/mL RTN was run in triplicate with each analysis (r^2=0.9999), employing a matrix of 50 mM maleic acid with 60 mM polyoxyethylene 10 lauryl ether (POE10) (pH 5.8) medium. Standards were obtained from a stock solution of RTN in methanol (1 mg/mL) by diluting 10-fold with the solubility media (i.e. matrix). Standards for each media were diluted with mobile phase to prepare the 0.78, 1.56, 3.125, 6.25, 12.5, 25 and 50 µg/mL concentrations. LOD and LOQ values were 0.004983 µg/mL and 0.0151 µg/mL.

2.13 Statistical Analysis

Studies were performed with triplicate. Regarding tablet formulation studies, data was analyzed using one-way analysis of variances (ANOVA) at the level of $p \leq 0.05$, and the significance of main effects and their interactions on tablet properties at the 95% confidence level were evaluated.

3 RESULTS AND DISCUSSION

3.1 Evaluation of true density and microscopy analysis

True density (ρ_t) can impact mechanical properties and compaction behaviors of powders, and σ_t influences porosity which affects tabletability (Elsergany et al., 2023). The true densities of RTN-SDD powders prepared at 70°C and 140°C were 1.318±0.008 g/cm^3 and 1.380±0.055 g/cm^3. These values were similar to, and perhaps slightly lower than, the true density of RTN and HPMCAS-L physical mixtures (1.391±0.001 g/cm^3). While true densities were similar for all powders, a perhaps slight decrease in true density after spray drying may reflect the loss of crystallinity, yielding higher ρ_t due to a more efficient arrangement of molecules in crystals (Honick et al., 2020a). Also, the true density of the blend powder (i.e. SDD powder from 70 °C inlet, MCC, CCS and MgS) was 1.4991±0.0028 g/cm^3. The true density of the blend granules (i.e. SDD powder from 70 °C, MCC, CCS and MgS after the crushing tablets compacted at 14kN and then sieving) was 1.3685±0.0005 g/cm^3.

For HPMCAS-H:L polymer, the true densities of the RTN-SDD powders prepared at 70°C and 140°C were 1.307±0.006 g/cm^3 and 1.403±0.067 g/cm^3, respectively and there was no significant difference ($p < 0.05$). For SoluPlus polymer, the true densities of the RTN-SDD powders prepared at 70°C and 140°C were 1.232±0.005 g/cm^3 and 1.263±0.024 g/cm^3, respectively and there was no significant difference ($p<0.05$). For PVP-VA polymer, the true densities of the RTN-SDD powders prepared at 70°C and 140°C were 1.271±0.003 g/cm^3 and 1.280±0.006 g/cm^3, respectively and there was no significant difference ($p<0.05$).

Figure S1 shows SEM images of coarse powder of RTN, physical mixture (20:80% w/w) of RTN and polymers (HPMCAS-L, HPMCAS-L:H, SoluPlus and PVP-VA), and SDD powders prepared at two different inlet temperatures. The coarse RTN particles were irregularly shaped particles at micrometer size. From images of the physical mixtures, RTN particles adsorbed onto the polymer particles. Meanwhile, SDD powders appeared as partially collapsed spheres with a fibrous surface. SDD powder shape reflects the rapid evaporation of solvent during spray drying. The collapsed spherical shape may also be related to the 20% drug load. Yu et al. observed SDD powders with 50% drug load showed round spheres, while SDD powders with 10% drug load showed wrinkled spheres. In Figure S1, more spherical particles were observed from 140 ˚C inlet temperature than from 70 ˚C; however, fiber-like structures appeared on the surface of the HPMCAS polymers, aggregating particles. This fibrous structure may reflect melted RTN at the higher inlet temperature, providing some connections between particles.

The formation of collapsed hollow spheres is related to the droplet drying mechanism of film-forming polymers and solvent pressure in the droplet. The solvent diffusion and evaporation rate can decrease when polymer solubility at the interface is surpassed; a viscous skin forms on the droplet. Spherical shapes indicate a high solvent partial pressure within the droplet, whereas a collapsed sphere structure likely arises from a

lower internal solvent partial pressure, leading the particle to fold inward (Ekdahl et al., 2019; Vehring, 2008; Yu et al., 2024). Hence, particle shape differences across the two different inlet temperatures (i.e. more spherical particles with 140 ˚C) reflect the differing solvent diffusion and evaporation rates, and different partial pressures, in the droplets.

3.2 Optimization of tablet formulation parameters in study 1

Study 1 results are summarized in Table S3, where there were three main effects studied: inlet temperature, SDD powder level, and disintegrant level. From multivariate analysis of the 2^3 experimental design, the main effects of all three parameters were significantly ($p \leq 0.05$) impacted: each tablet thickness, hardness, and disintegration time. Meanwhile, all two-way interactions (e.g. SDD powder level - disintegrant level interaction) and the three-way interaction were significant for disintegration only. Model r^2 was 0.9945 for thickness, 0.9903 for hardness, and 0.9998 for disintegration time, indicating model was able to explain observations.

3.2.1 Effect of study 1 parameters on tablet thickness

Figure 3 are the 3D surface graphs of study 1 parameter effects on tablet thickness, where direct compression was performed using 1 kN. Tablet thickness decreased when inlet temperature decreased and SDD powder level increased, independently from disintegrant level. This sensitivity to SDD powder level was greater for the higher inlet temperature, perhaps due to bulk powder density. The bulk density of the RTN-SDD powder from 140°C (i.e. 0.082±0.002 g/cm^3) was markedly lower than that from 70°C (i.e. 0.251±0.003 g/cm^3). In the literature, bulk density decreased for higher drying temperature (Tao et al., 2024). This relationship may indicate an elevated evaporation rate aimed at lowering the moisture content of the powders, potentially influenced by the formation of a porous or fragmented structure in the dried product (Walton, 2000).

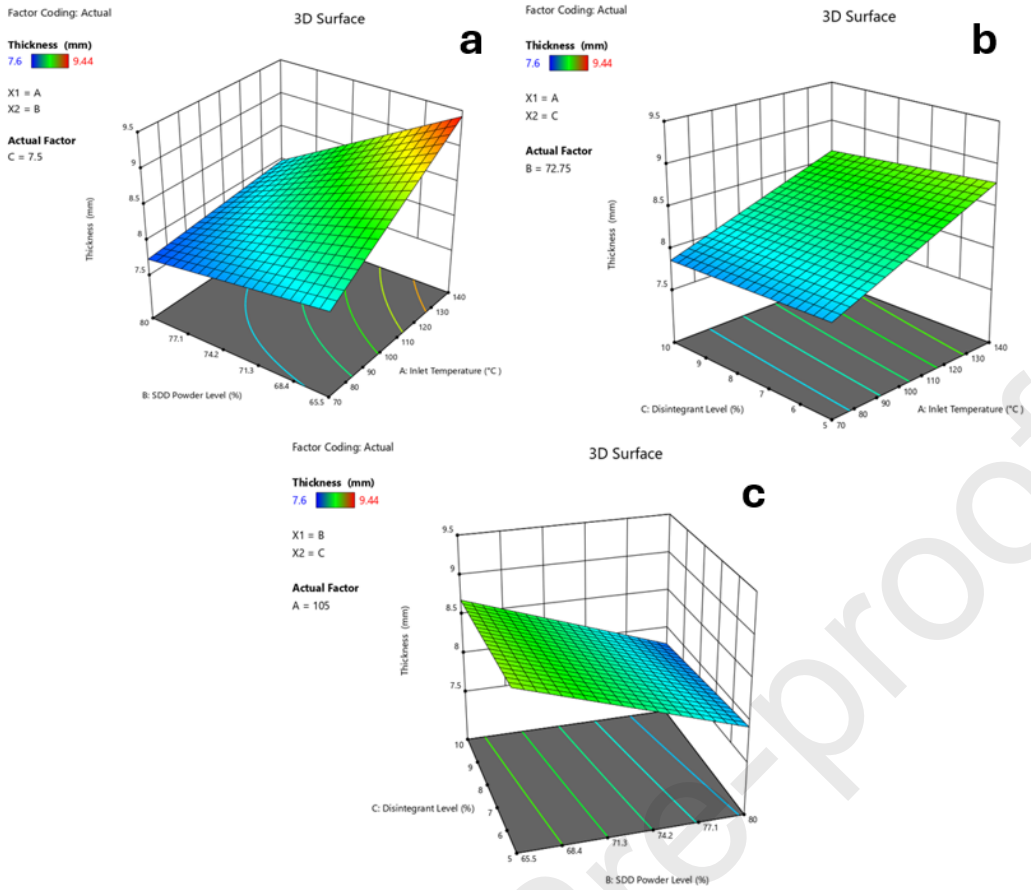

Figure 3. 3D surface graphs showing the effect of study 1 parameters of inlet temperature, SDD powder level, and disintegrant level on tablet thickness.

3.2.2 The effect of study 1 parameters on tablet hardness

Figure 4 are 3D surface graphs of study 1 parameter effects on tablet hardness. Tablet hardness decreased when inlet temperature decreased and SDD powder level increased independently from disintegrant level. These results are consistent with SEM images, where fiber-like structures on polymer surface and aggregated particles from 140 °C inlet temperature. RTN's melting point is 128.21 °C (Oktay and Polli, 2024), such that RTN melted when inlet temperature was 140 °C, causing bridging particles. Also, hardness decreased when SSG level increased. Demina et al. observed hardness decreased from 76.2 N to 47.6 N when SSG increased from 2% to 6% (Demina et al., 2018). SSG's irregular shape may underpin this decrease in tablet hardness.

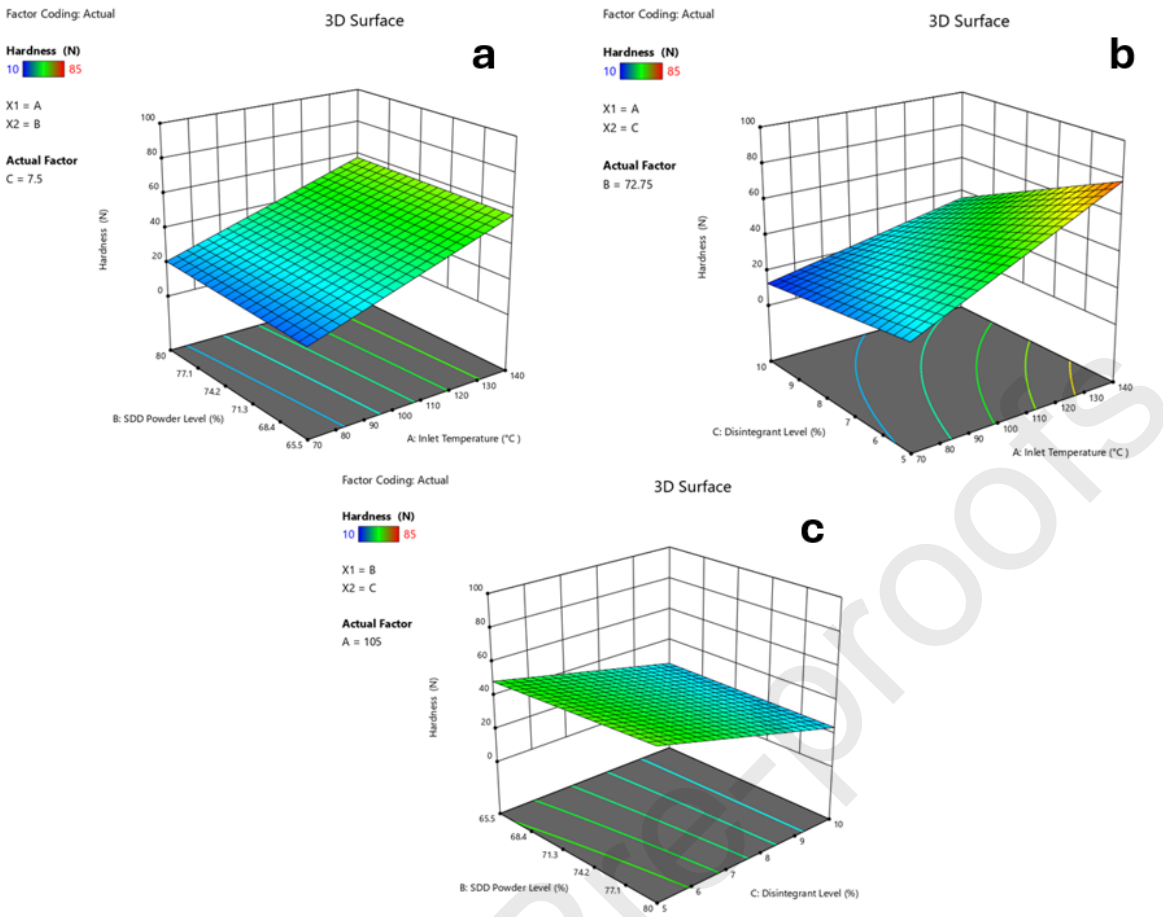

Figure 4. 3D surface graphs showing the effect of study 1 parameters of inlet temperature, SDD powder level, and disintegrant level on tablet hardness.

3.2.3 The effect of study 1 parameters on tablet disintegration time

Figure 5 are 3D surface graphs of study 1 parameter effects on disintegration time. Disintegration time decreased when inlet temperature decreased and SDD powder level increased, independently from disintegrant level. Also, disintegration time was decreased when disintegrant level increased. SSG is a swelling disintegrant(Demina et al., 2018).

From study 1, optimum parameters were use of 70 °C of inlet temperature to fabricate SDD powder, 65.5 % SDD powder level, and 10 % disintegrant level to obtain tablets with smaller thickness, lower hardness, and faster disintegration. These parameter levels were used in study 2.

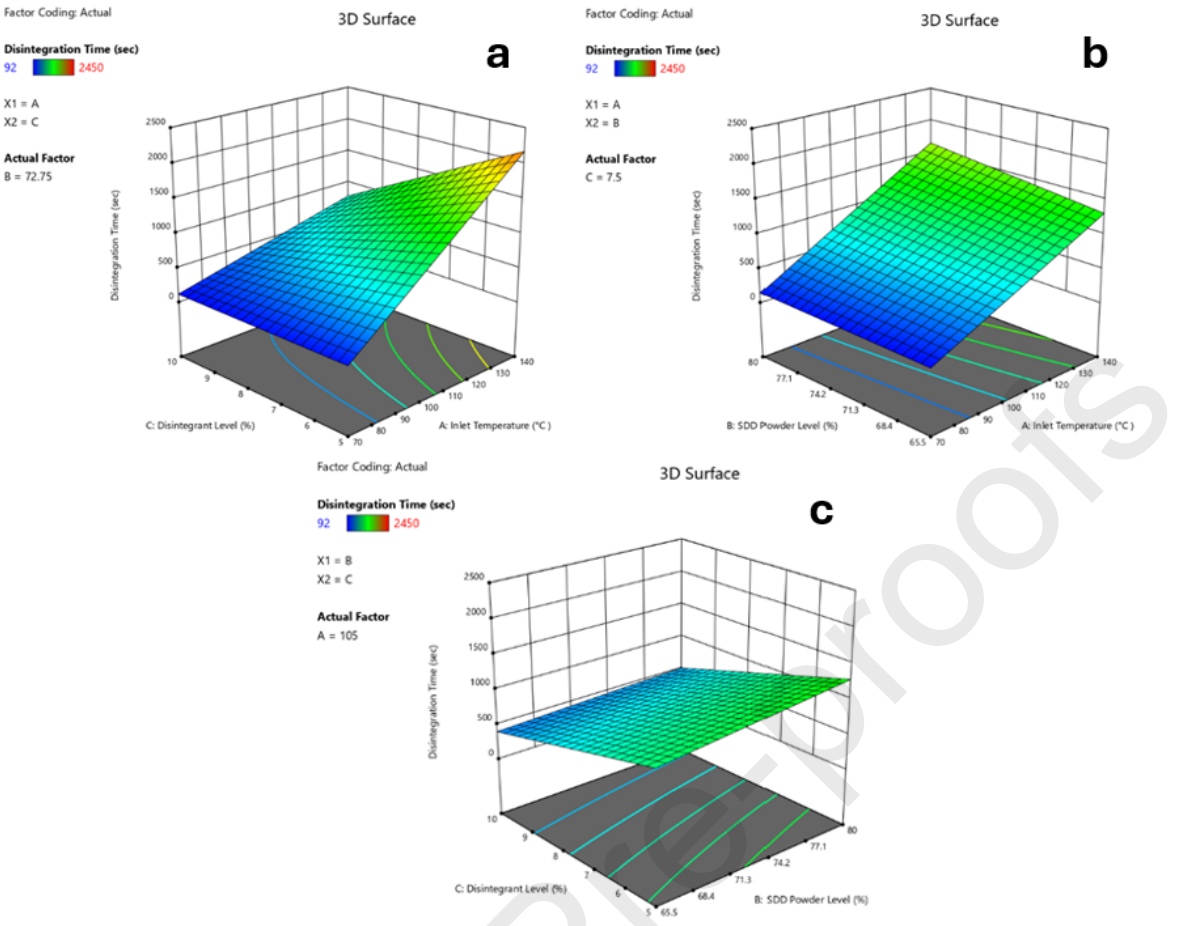

Figure 5. 3D surface graphs showing the effect of study 1 parameters of inlet temperature, SDD powder level, and disintegrant level on disintegration time.

3.3 Optimization of tablet formulation parameters in study 2

Study 1 results are summarized in Table 1, where there were two main effects studied across six formulations: filler type and disintegrant type. Tablets compacted via direct compression using 1 kN. There was no significant difference in tablet thickness, length or width. Most notable, the combination of MCC and CCS provided tablets with the most rapid disintegration.

Table 1. Tablet thickness, lengths, width, hardness and disintegration time from study 2. Formulations varied in fillers (MCC or DCP) and disintegrant (SSG, CCS, and CP). Most notable, the combination of MCC and CCS provided tablets with the most rapid disintegration.

Filler Type	Disintegrant Type	Thickness (mm)	Length (mm)	Width (mm)	Hardness (N)	Disintegration Time (sec)
MCC	CP	7.91±0.01	19.07±0.01	10.11±0.01	19.7±0.9	162.3±1.8

MCC	SSG	7.97±0.02	19.03±0.01	10.12±0.03	12.3±0.3	97.3±0.9
MCC	**CCS**	**8.08±0.01**	**18.97±0.02**	**10.09±0.01**	**8.0±0.6**	**54.7±1.8**
DCP	CP	7.81±0.01	19.04±0.01	10.10±0.01	19.3±1.2	152.7±4.3
DCP	SSG	7.87±0.07	18.98±0.03	10.06±0.01	14.3±0.9	115.7±11.0
DCP	CCS	8.05±0.04	19.03±0.01	10.13±0.03	10.0±0.6	90.3±1.2

3.3.1 Effects of study 2 parameters on tablet dissolution

Figure 6 plots dissolution profiles from study 2. All tablets showed immediate release profile and reached over 99% RTN release by 360 min, except the tablet containing dicalcium phosphate (DCP) and sodium starch glycocholate (SSG) (97.8±0.9%). At 60 min, the tablet containing MCC and CCS provided the highest release (79.5±5.6%). The lowest (31.6±1.2%) used DCP-CP (Table S4). At 60 min, the rank order was: MCC-CCS > DCP-CCS > MCC-SSG > DCP-SSG > MCC-CP > DCP-CP. MCC always showed faster profile than corresponding DCP formulation. Also, formulations also followed CCS > SSG > CP.

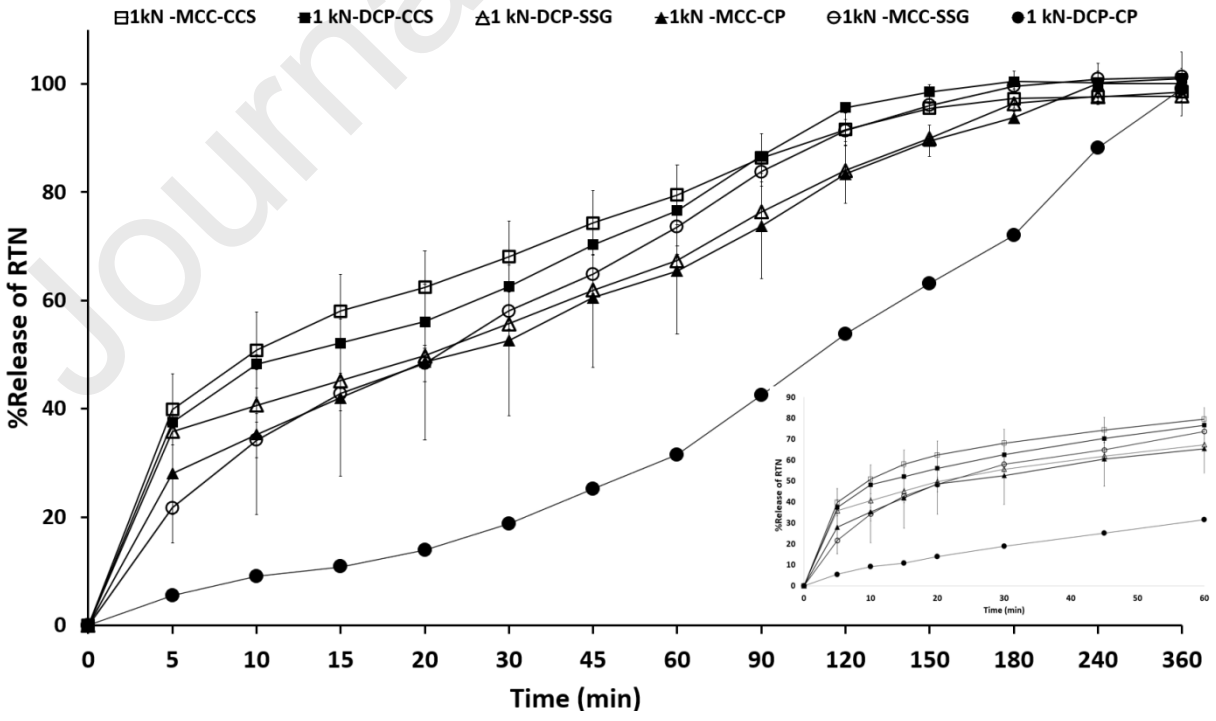

Figure 6. Dissolution profiles from study 2, where filler type and disintegrant type were varied. Fillers were MCC and DCP. Disintegrants were SSG, CCS, and CP.

Dissolution profile was analyzed and compared via area-under-the-dissolution-curve (AUC) calculations. Table S4 shows AUC values for (i.e. up to) 60 min and 360 min . AUC values from 0-360 min were indistinguishable from one another and not significant difference ($p>0.05$), in part since all tablets were essentially completely dissolved. Meanwhile, $AUC_{(0\text{-}60\ min)}$ values differed and were 710±10, 1720±310, 1960±360, 1560±280, 1800±280 and 2020±320 μg.min/mL for DCP-CP, DCP-SSG, DCP-CCS, MCC-CP, MCC-SSG and MCC-CCS, respectively. The highest AUC value involved tablets containing MCC and CCS, while the lowest involved tablets containing DCP and CP.

Hence, MCC and CCS were selected as the filler and disintegrant for process optimization in study 3. Al-Ibraheemi et al. observed advantages of MCC due to MCC's excellent filler and compaction properties for ASDs (e.g. highly plastic and possessing a low elastic energy) and favorable tableting characteristics (Al-Ibraheemi et al., 2013).

Regarding CCS, Zhang et al. also observed the rank order performance of disintegrants to be CCS > SSG > CP for disintegration of spray dried amorphous solid dispersion tablets, as found here for disintegration and dissolution. This performance reflects mechanisms of the disintegrants. Croscarmellose sodium and sodium starch glycolate are disintegrants based on sodium salts, primarily facilitating tablet disintegration through swelling—characterized by three-dimensional expansion upon hydration. In contrast, crospovidone is a non-ionic disintegrant that acts predominantly via shape recovery, involving uniaxial expansion as the polymer particles return to their original form upon contact with water (Zhang et al., 2024). Bauhuber et al. also observed CCS was preferred over SSG and CP for tableting of a hydrophobic drug (Bauhuber et al., 2021). The slower disintegration profile provided by CP may be related to CP's larger particle size of about 125 μm, compared to CCS and SSG (about 40μm) (JRSPharma, 2020). An increase in particle size may lead to greater spacing between the relatively few large crospovidone (CP) particles. Additionally, the limited swelling capacity of these larger particles may hinder the formation of a continuous network of hydrated particles, thereby restricting effective liquid transfer between them (Bauhuber et al., 2021).

Collectively, study 1 and 2 identified the following optimum formulation parameters: 65.5% SDD powder level, 24% MCC, and 10% CSS. Also, the RTN/HPMCAS SDD should be fabricated using 70^{o}C inlet temperature.

3.4 Optimization of tablet process parameters in study 3

Table 2 lists in-die porosity (%), Heckel in die value (Ln(1/(1-D))), and tensile strength of tablets prepared by direct compression and dry granulation. In each process, compaction force was varied.

For direct compression, compaction force was 1, 2, 4, 7, or 14 kN and were converted to compaction pressure by considering tablet surface area of 171.39 mm^2. Compaction pressures were in the range of 5-100 mPa. Tablet porosity was calculated by considering tablet weight and volume, and true density of the blend powder. Across all compaction forces, the powder amount in each die was the same, so tablet weight was

the same across all compaction forces. While tablet weight (about 763,64 mg) and true density (1.4991 g/cm^3) were same across tablets, tablet volume changed due to differing compaction forces. As expected, tablet porosity decreased with increasing compaction forces. Increasing compaction force 1 kN to 17 kN resulted in tablet volumes to decrease from 1.109±0.001 cm^3 to 0.614±0.003 cm^3. The lowest porosity of 17.08±0.47% was from 17kN, while highest porosity of 54.23±0.05%) was from 1kN.

Table 2 also shows Heckel analysis results. The Heckel equation describes the relationship between relative density and porosity, based on the assumption that powder densification during compaction follows the kinetics of a first-order chemical reaction (Heckel, 1961; Wang et al., 2021). Literature evidence supports the equivalence of the in-die and out-of-die methods, indicating that the in-die approach is comparably suitable for evaluating powder compressibility (Berkenkemper and Kleinebudde, 2022). Heckel in die values increased from 0.612 to 1.768 with greater compaction pressure from 5.776 to 99.459 mPa. Higher compaction force provided higher compressibility and greater elastic deformation. Tablet tensile strength is important mechanical integrity during transport and handling. Elevated compaction force (from 1kN to 17 kN) and pressures (from 5.776 to 99.459 mPa) increased tensile strength (from 0.029 to 2.430 mPa).

Table 2. Tablet properties in study 3 using direct compression and dry granulation. Compaction force was varied.

	Compaction force (kN)	Mean compaction force (kN)	Mean compaction pressure (mPa)	In die porosity (%)	Heckel in die	Tensile strength (mPa)
Direct compaction	1	0.990±0.021	5.78±0.12	54.2±0.1	0.612±0.001	0.029±0.002
	2	2.01±0.01	11.7±0.1	49.2±0.1	0.700±0.001	0.109±0.009
	4	4.08±0.01	22.8±0.1	38.9±0.2	0.944±0.005	0.232±0.006
	7	7.02±0.01	41.0±0.1	27.5±0.5	1.29±0.02	0.743±0.062
	14	14.06±0.02	82.0±0.1	20.0±0.4	1.61±0.02	1.90±0.07
	17	17.05±0.02	99.5±0.1	17.1±0.5	1.77±0.03	2.41±0.03
Dry Granulation	1	0.953±0.009	5.56±0.05	49.9±0.1	0.696±0.001	0.029±0.002
	2	1.93±0.02	11.2±0.2	43.5±0.7	0.833±0.017	0.061±0.003
	4	3.83±0.05	22.3±0.3	36.0±0.4	1.02±0.01	0.123±0.006
	7	6.75±0.03	39.4±0.2	25.9±0.7	1.35±0.03	0.316±0.024
	14	13.96±0.07	81.5±0.4	18.7±0.4	1.68±0.02	0.757±0.018
	17	16.80±0.04	98.1±0.2	12.8±0.7	2.06±0.06	1.21±0.02

Similar results were observed for the dry granulation method, which employed a 14kN pre-compaction force. In Table 2, compaction pressure ranged from 5.556±0.051 mPa to 98.098±0.203 mPa from 1, 2, 4, 7, 14, 17 kN of compaction forces. The tablet surface area was 171.39 mm^2. Total granule weight in each die (about 763,64 mg) was constant, like for the direct compaction method. For the porosity calculations, the true density of blend granules was 1.3685±0.0005 g/cm^3. When the compaction force

increased from 1kN to 17 kN, table volume decreased from 1.109±0.001 cm^3 to 0.638 ±0.005 cm^3. Correspondingly, tablet porosity decreased with compaction force (Khan and Musikabhumma, 1981; Yu and Hoag, 2024). The lowest and highest porosities were 12.77±0.72% and 49.86±0.06% at 1kN and 17 kN, respectively. These values were lower than that of tablets prepared from direct compression. As compaction force increased, granule fragmentation became more pronounced, enhancing interparticle interlocking. The resulting smaller fragments effectively occupied the voids between larger particles, leading to reduced bed and tablet porosity (Markl and Zeitler, 2017; Omar et al., 2015; Wang et al., 2021). Heckel in die and tensile strength showed similar results to the direct compaction method. Both are increased with an increase in compaction force and pressure, yielding higher compressibility and mechanical integrity. Yield pressure was also found lower for dry granulation than direct compaction method. While the yield pressure (Py) value from direct compression was 82.05 MPa, Py was 76.23 MPa for dry granulation. Py is the inverse of K (slope of the Heckel Equation) and it is the pressure at which a material begins to undergo plastic deformation (Honick et al., 2020b).

For all compaction forces, tablet porosity and Heckel in die values were lower from direct compression than dry granulation (Figure 7 a-b). Meanwhile, tensile strength was higher for direct compression than dry granulation (Figure 7c). There was more space between granules compared to the powders, so the structure from dry granulation was more porous and more accommodating for compression. However, greater porosity caused lower tablet mechanical strength (Figure 7d), similar to the literature (Honick et al., 2020b)

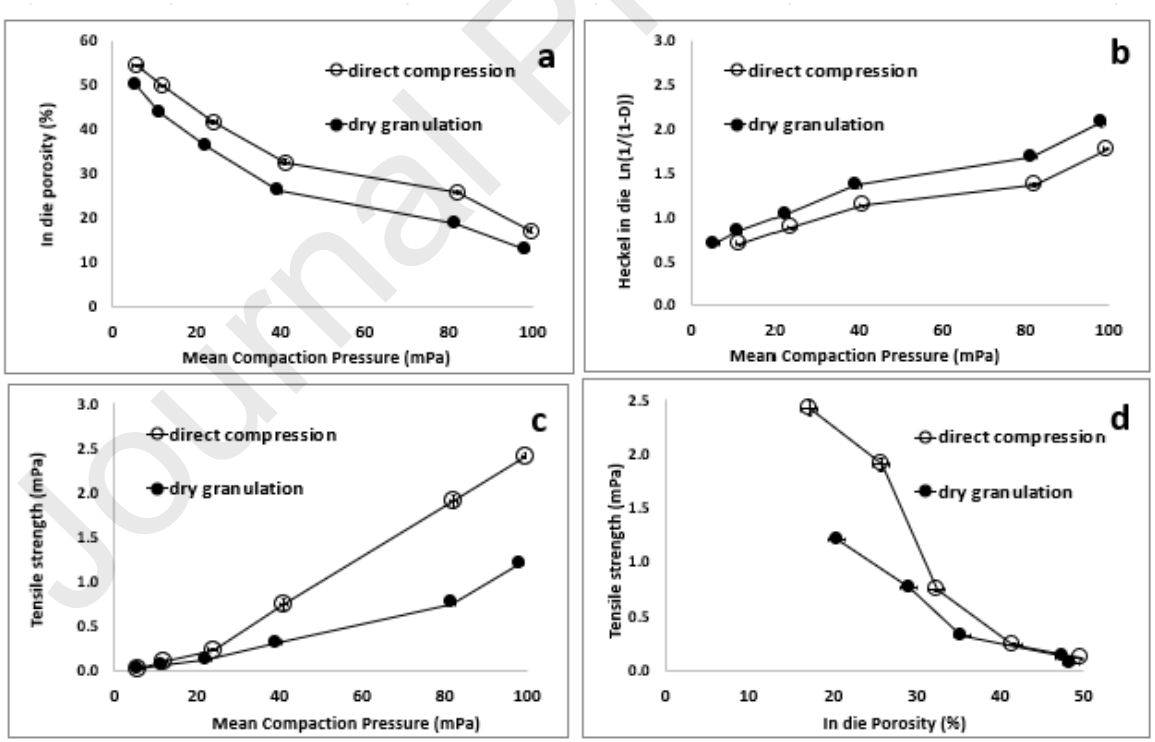

Figure 7. The representative plots of in die tablet porosity % (a), Heckel in die (b) and Tensile strength (b) versus mean compaction pressures (mPa), and tensile strength versus in die porosity% values of tablets (d). Data indicates mean±SEM (n=3)

3.4.1. The effect of the process parameters in study 3 on dissolution

To assess the effect of manufacturing process and compaction pressure on tablet dissolution, dissolution was performed at 37 °C in modified compendial media (i.e. maleic acid buffer with 60 mM POE, pH 5.8). Figure 8 plots dissolution results. For direct compression, RTN release interestingly increased when compaction force (i.e. rank order 7kN > 4kN > 2kN > 1kN). This rank order reflects the need for sufficient solid fraction for efficient wetting and disintegration. For dry granulation, with 14kN pre-compaction force, dissolution favored 7kN, with rank order was 7kN > 4kN > 14kN > 17kN. Force less than and more than 7kN decreased release rate. Figure 8 plots dissolution results. For direct compression, RTN release interestingly increased with compaction force (i.e. rank order 7kN > 4kN > 2kN > 1kN). For dry granulation, with 14kN pre-compaction force, dissolution favored 7kN, with release rate rank order 7kN > 4kN > 14kN > 17kN; force less than 7kN and more than 7kN decreased release rate. Of note, all RTN tablets here contained HPMCAS-L, MCC, CCS, and MgS. Other stuides have previously observed a higher tablet compaction force to result is more rapid dissolution (Adeleye, 2019). Contributing factors include particle bonding and pore structure impacts.

Two possible explanations for tablets here to show higher dissolution when compaction force increased to 7kN concern HPMCAS-L brittle fracture and pore structure effects. HPMCAS-L SDDs are brittle (Honick et al., 2020a; Iyer et al., 2013; Sauer et al., 2021). HPMCAS-L brittle fracture appears to contribute to the observed dissolution pattern. As previously observed for lactose monohydrate, higher compaction of HPMCAS-L caused greater brittle fracture and more HMPCAS-L surface area formation, which promoted dissolution (Sagiraju et al., 2024). Here, 7kN was the highest compaction force evaluated in direct compression and resulted in the fastest dissolution. Interestingly, higher compaction beyond 7kN (e.g. 12kN) for dry granulation slowed dissolution, with 7kN being the most rapid. Of note, Skelbæk-Pedersen et al. studied dry-granulated lactose/MCC granules and observed that granule fragmentation was largely confined to less than about 10 MPa, after which plastic densification predominated. Hence, beyond modest forces, compact microstructure (e.g. porosity) and liquid transport, and not continued fragmentation, slowed disintegration. This trend, where dissolution increased with compaction force up to an optimal point, has also been observed in studies on wet-granulated paracetamol tablets (Pan et al., 2015).

Also, of perhaps secondary consideration, low compaction force resulted in high porosity, where MgS film effect appeared to dominate CCS wetting functioning. MgS is a plate-like, hydrophobic material, which can coat particles and reduce dissolution (Ariyasu et al., 2016; Vaithianathan et al., 2016; Zarmpi et al., 2020). At high porosity, pores are larger such that there appears to be greater air entrapment, and MgS's hydrophobic film effect attenuated CCS's ability to wick water and swell.

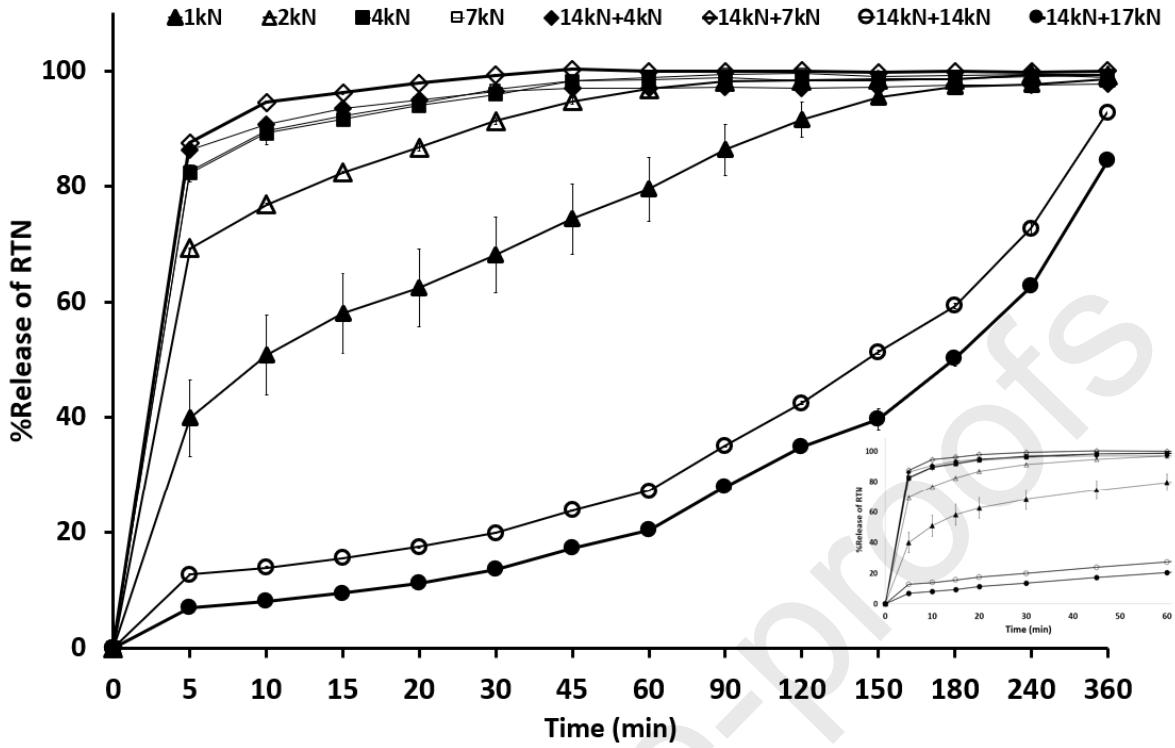

Figure 8. Interplay of process method and compaction force on RTN dissolution. Inset plot shows dissolution for only the first 60 min. Tablets were fabricated via both direct compression and dry granulation. In figure, the four formulations made via dry granulation include the pre-compression force of 14kN in label.

In Figure 8, drug release reached to 99-100% in 360 min for all tablets except those dry granulation tablets compressed using 14kN (92.8±1.2%) and 17kN (84.5±0.8%). Table 3 lists dissolution AUC values until 60 min, with dry granulations yielding both the fastest and slowest tablets. Across tablets from both direct compression and dry granulation, rank order was 14kN+7kN > 7kN > 4kN > 14kN+4kN > 2kN > 1kN > 14kN+14kN > 14kN+17kN. The highest AUC value observed for tablets prepared with 14kN+7kN was 2750 µg.min/mL.

Tablet 3 lists tablet hardness and thickness, as well as percent dissolved at 60 min. In USP monograph <1217>, the acceptable limits of hardness are 5–8 kgf, which equates to 49 N-78.5N (Dulla et al., 2018; Karmakar and Kibria, 2012; Monographs, 2009a, b). Only tablets prepared from direct compression using 4 kN and tablets prepared from dry granulation using 14 kN+7kN were acceptable (i.e. within acceptable hardness range). The hardness of the tablets prepared with 14+7 kN was 56.0N which meet the USP specification (United States Pharmacopeia, 2012). The optimum process was concluded to be dry granulation using 14+7 kN, considering it provided the fastest dissolution and acceptable hardness.

Interestingly, dissolution reflected tablet hardness, an indicator of tablet solid state arrangement, although qualitatively differed for direct compression and dry granulation. Of note, the two process methods employed different ranges of applied compaction forces. For direct compression, compaction force less than 4kN resulted in slower

dissolution. Meanwhile, for dry granulation, compaction force higher than 4kN and 7kN resulted in slower dissolution.

Table 3. Effects of tablet compaction force on RTN tablet properties for direct compression and dry granulation.

Compaction force (kN)	Hardness (N)	Thickness (mm)	% drug release at 60 min	$AUC_{0\text{-}60\ min}$ (µg.min/mL)
1kN	7.00±0.58	8.07±0.02	79.5±5.6	2020±320
2kN	23.7±0.9	7.61±0.01	96.9±0.5	2640±530
4kN	46.0±1.2	6.59±0.01	98.5±0.4	2710±550
7 kN	132±11	5.93±0.01	98.9±0.2	2710±540
14kN +4kN	22.3±1.2	6.08±0.03	97.0±0.1	2690±540
14kN +7kN	56.0±4.0	5.91±0.01	99.9±0.2	2750±550
14kN +14kN	151±2	5.36±0.02	27.2±0.1	666±119
14kN +17kN	191±3	5.29±0.01	20.4±0.4	481±80

3.4.2.Comparison of dissolution profiles of optimized tablet formulation with same formulation but with higher inlet temperature

As described above, the optimum tablet employed SDD fabricated using 70°C inlet temperature. Figure 9 plots the dissolution profile from the optimum tablet, along with a tablet made the same way, but from SDD fabricated with HPMCAS H:L, PVP-VA and SoluPlus polymers and as well as with inlet temperature of 140°C. In Fig. 9, complete release (i.e. 100mg/900ml or 111 µg/mL) is well above the RTN's amorphous solubility (~30 µg/mL) (Purohit and Taylor, 2017).

For HPMCAS-L polymer, the optimum tablet (i.e. with lower inlet temperature) exhibited faster dissolution. The percent RTN dissolved from tablets and corresponding f_2 comparison to Norvir tablet are shown in Table S5. In 60 min, the tablet containing SDD powders prepared at 70 °C released 99.9% of RTN, while the corresponding tablet containing SDD powders prepared at 140 °C showed 97.2% RTN dissolved. These values were 95.4% and 95.4% for PVP-VA polymer, 13.5% and 9.3% for SoluPlus polymer, 96.0% and 83.3% for HPMCAS H:L polymer at the 70 °C and 140 °C inlet temperature, respectively. In Table S5, every dissolution profile through 30 min was different from Norvir tablet, as perhaps is evident in Fig 9. For example, tablets with each HPMCAS-L and PVPVA (for both 70°C and 140°C inlet temperatures) were faster than Norvir tablet.

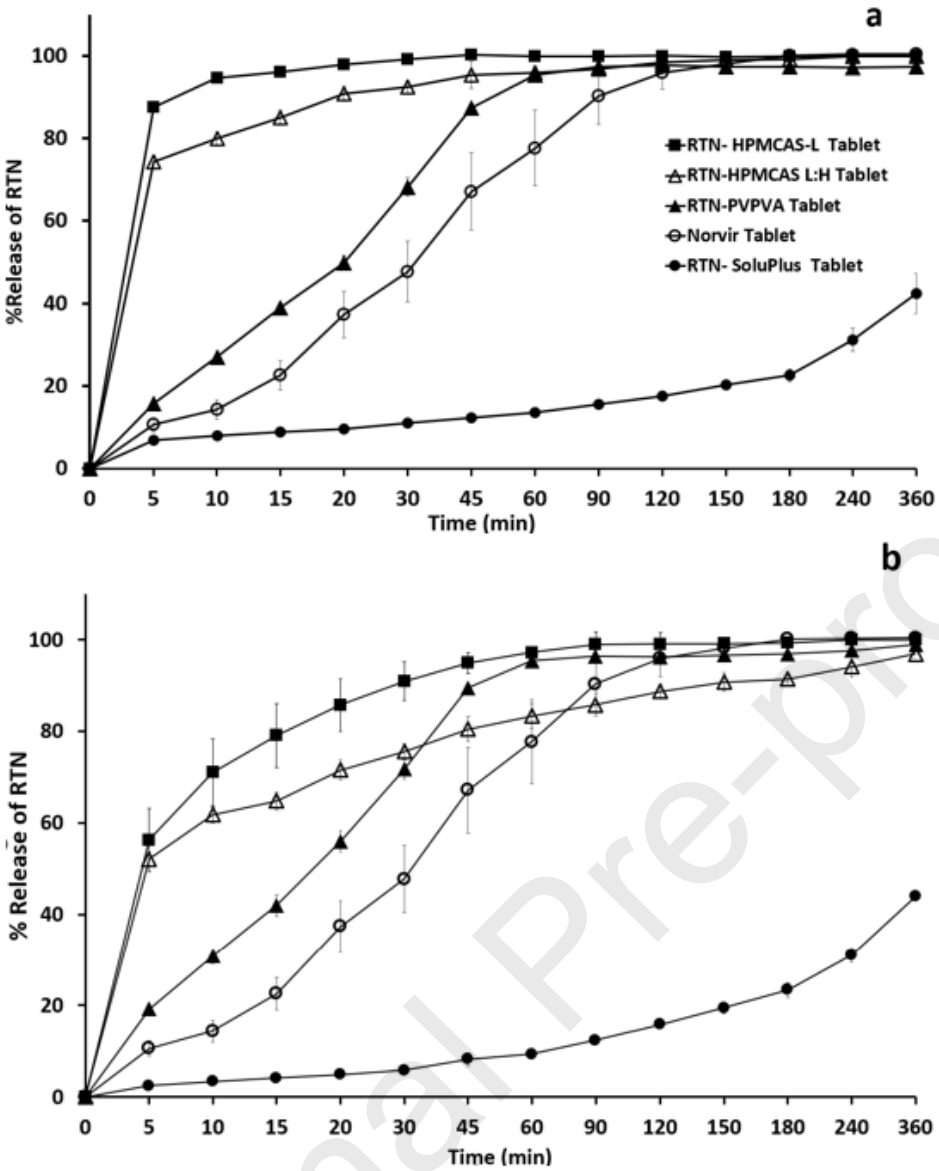

Figure 9. Dissolution profiles of optimum tablets with various polymers compared to the Norvir® tablet. Optimized tablets containing SDD fabricated using inlet temperature of 70°C (panel a), using inlet temperature of 140°C (panel b). The optimum RTN-HPMCAS-L tablet exhibited faster dissolution.

The AUC values of tablets were given in Table S6. AUC values in 60 min ($AUC_{0\text{-}60\ min}$) were highest for the HPMCAS-L polymer 2750 µg.min/mL and 2610 µg.min/mL for 70 °C and 140 °C, respectively. AUC values in 120 min ($AUC_{0\text{-}120\ min}$) were 5504.4 µg.min/mL and 5532.15 µg.min/mL for 70 °C and 140 °C, respectively. Assuming polymer is the major formulation contributor to ASD tablet performance, we had anticipated PVPVA as a potentially faster dissolving formulation (Ellenberger et al., 2018; Rosenberg et al., 2012; Simões et al., 2019). However, there are a limited number of studies that compare these two most common polymers for ASDs. Like results here, Purohit et al. also found that RTV HPMCAS ASDs showed faster dissolution than RTN PVP-VA ASDs (Purohit and Taylor, 2017). Moreover, Ellenberger et al. showed that RTV ASD using HPMCAS exhibited a higher release than Norvir in neutral pH 6.8 media (Ellenberger et al., 2018).

The tablets containing SDD prepared with higher inlet temperature showed slower dissolution since RTN melted, yielding bridging between polymer particles and higher tablet hardness (i.e. 95N for 140°C versus 56N for 70°C). Spray-drying HPMCAS at elevated inlet temperature (140°C) produced powders with markedly higher true density, SEM-visible fibrous surface networks, and slower dissolution compared with powders obtained at 70°C. These three observations are mechanistically linked through the thermal properties of HPMCAS. Among the polymers studied, HPMCAS has the highest T_g (~122°C) similar to literature (Friesen et al., 2008), which places it near the high spray drying temperature. Under 140 °C of inlet temperature, HPMCAS polymer chains exhibit increased mobility, allowing physical relaxation and partial coalescence. The observed fibrous, network-like structures on SEM images of SDDs containing HPMCAS polymers (Figure S1 panel d-e for HPMCAS-L and panel h-i for HPMCAS L:H) suggest that, as solvent evaporation continues and droplet temperature rises beyond T_g, chain entanglement and surface rearrangement occur (Corrie et al., 2023). The resulting surface densification is reflected in increased true density values (Section 3.1), indicative of reduced free volume and lower porosity. For HPMCAS, an enteric polymer whose dissolution requires hydration and erosion, the dense fibrous shell acts as a diffusion barrier, slowing medium penetration and delaying polymer erosion and drug release (Corrie et al., 2023; Friesen et al., 2008). In contrast, while PVP-VA and SoluPlus also exhibited higher density at 140°C, their greater intrinsic water solubility, hygroscopicity, and amphiphilic properties facilitate rapid water uptake and dissolution, thereby offsetting the effects of densification at 140°C (Alonzo et al., 2010; DiNunzio et al., 2008). Thus, the interplay of high T_g (thermal sensitivity near processing temperature), increased true density (reduced free volume), and fibrous shell morphology (diffusion barrier) provided for slower dissolution for HPMCAS formulations under high temperature spray drying.

3.5. D-HFM results of optimum tablet

Figure 10 plots the D-HFM permeation profile of RTN from optimum tablet, as well as the HFM profile from RTN solution. About twice as much RTN permeated (i.e. crossed the HFM module) from the solution than from the HPMCAS-L tablet. Figure S2 and Figure S3 show the percent RTN dissolved and remaining in the donor compartment for HPMCAS-L tablet and RTN solution, respectively. Dissolution of the tablet was rapid (Figure S2 and S3). The main observation from the permeation profiles in Figure 10 was that % permeated amount of RTN from HPMCAS-L tablet was about half that of solution (i.e. P_{app} = 3.90x10^{-6} cm/sec for HPMCAS-L tablet versus 9.30x10^{-6} cm/sec for solution). % permeated amount of RTN from PVP-VA (i.e. P_{app}= 10.2±0.60 cm/sec) and Norvir tablet (i.e. P_{app}= 14.7±8.46 cm/sec) was similar to RTN solution (Table 4).

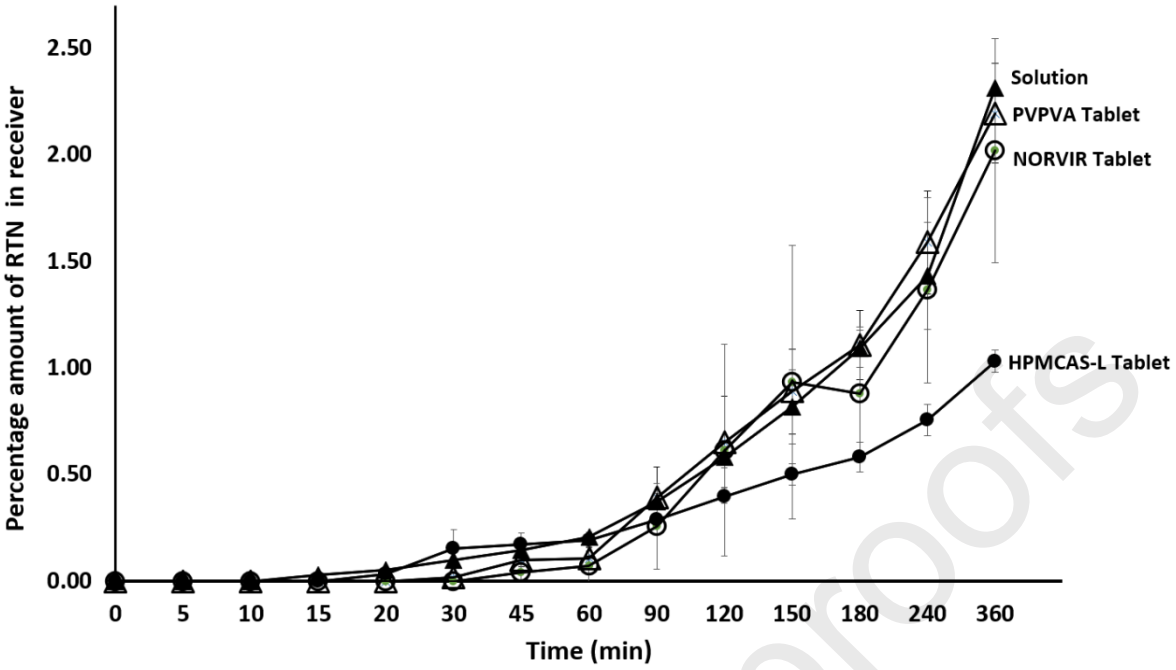

Figure 10. D-HFM permeation profiles of RTN tablets with various polymers. About 1% of drug dissolved and permeated from the HPMCAS-L tablet over 360 min. Also shown is RTN permeation profile from solution, where about 2% of drug permeated, similar to the PVP-VA polymer tablet and Norvir® tablet. Each tablet and solution contained 100 mg RTN.

Firstly, the P_{app} from tablet and solution of $3.90x10^{-6}$ cm/sec and $9.30x10^{-6}$ cm/sec, respectively, were several fold lower than previously observed HFM and D-HFM P_{app} about 50 x 10^{-6} cm/sec (Adhikari et al., 2022a). These higher P_{app} were from more simple formulations and presumably reflect the permeability of free drug across HFM. However, RTN here was formulated as an ASD, including from the so-called solution study, where Norvir powder, employing PVP-VA as a polymer, was used to fabricate a "solution". RTN release from PVP-VA ASD is known to result in droplets of RTN via liquid-liquid phase separation (LLPS) of drug and polymer (Men and Polli, 2024). That is, RTN release does not result in molecularly dissolved RTN, at least not immediately. For each tablet and solution, their low P_{app} is consistent with ASD release resulting in drug-rich droplets from LLPS of drug and polymer.

Secondly, P_{app} from tablet (i.e. RTN/HPMCAS-L ASD) being lower than P_{app} from solution (i.e. RTN/PVP-VA ASD) suggests that the drug-rich droplets from HPMCAS-L resulted in less molecularly released RTN than from PVP-VA. This assumes that molecularly solubilized RTN is the main form of drug that can flux across the HFM. Alternatively, the main form of RTN permeation across HFM was drug colloid (e.g. drug-rich droplets, or colloid the result of both ASD release and incorporation of POE from donor media). Given the HFM membrane pore size was 300 kDa, which we estimate to provide a pore size greater than 60 nm, this alternative permeation model would require the drug-containing colloid from PVP-VA to be smaller than drug-containing colloid from HPMCAS-L. A third model is colloid schuttling (or micelle schuttling) as the main permeation mechanism (Patel et al., 2025). However, the complexity of this mechanisms is not amenable to data analysis here.

D-HFM results in Fig. 10 insipred the measurement of colloid size from dissolving RTN/HPMCAS-L SDD and RTN/PVP-VA SDD. Figure 11 panel A shows mean colloid

size of RTN/HPMCAS-L SDD and RTN/PVP-VA SDD in the disolution media with 60mM POE10. The very high amount of surfactant dominated and was the only observable colloid, with a size of about 8nm. Hence, colloid size was not able to explain the difference in HFM permeation performance between RTN/HPMCAS-L ASD and RTN/PVP-VA ASD.

Figure 11 panel B shows mean colloid size of RTN/HPMCAS-L SDD and RTN/PVP-VA SDD in the disolution media without 60mM POE10. At the early timepoints (e.g. 5 and 15 min), RTN/HPMCAS-L was about twice as large as RTN/PVP-VA. By 30min, collloid size of RTN/PVP-VA declined markedly, while RTN/HPMCAS-L size continued to increase Between 60-360min, RTN/HPMCAS-L declined, while RTN/PVP-VA inceased and then decreased. A complicating factor in examining Fig 11 is that, while these colloids reflect LLPS above RTN's amorphous solubility, these colloids may or may not be a dominate form of RTN.

Shetty et al. also assessed the impact of each PVP-VA and HPMCAS on the dissolution behavior and diffusive flux of GDC-6893 ASDs. For 20% drug-load, ASD containing HPMCAS polymer had lower flux compared to the PVP-VA at 100 µg/mL. These HPMCAS ASD also had much larger colloid particle size than PVPVA ASD (i.e. 444 nm versus 87 nm) (Shetty et al., 2025). Of note, Indulkar et al. conducted dissolution on RTN/PVPVA ASD (with 10% drug load) and observed LLPS colloids with mean size of 218nm (Indulkar et al., 2019) at 30 min. Dhumal et al. conducted dissolution on itraconazole ASDs with HPMCAS-L (with 20% drug load) and observed LLPS colloids with mean size of about 250nm from 10-90 min (Dhumal et al., 2024).

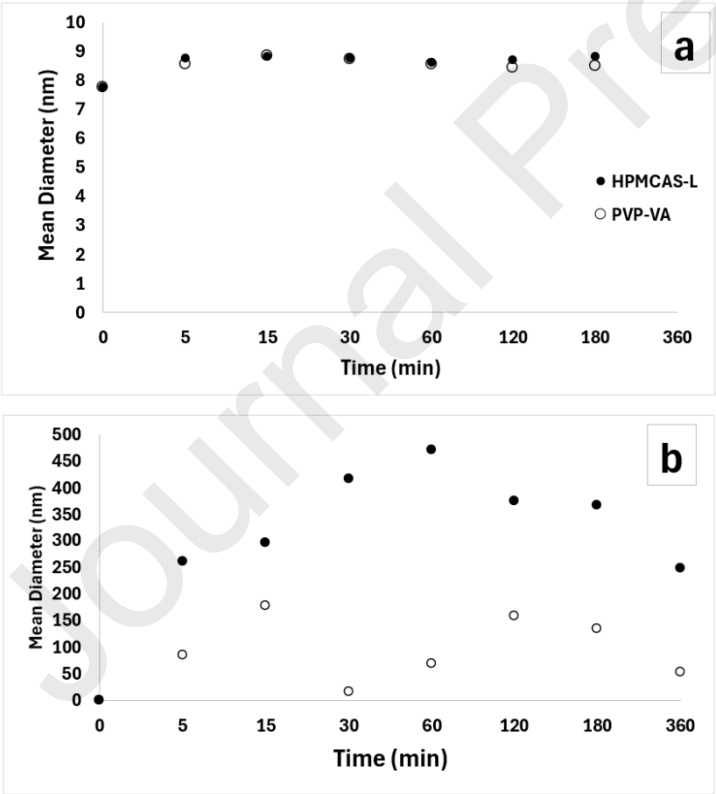

Figure 11. Dynamic light scattering results of in vitro powder dissolution of samples RTN/HPMCAS-L SDD and RTN/PVP-VA SDD. Dissolution media was maleic acid buffer (pH 5.8) with 60 mM POE in panel A, and without 60 mM POE in panel B. In panel A, colloid size was always about 8nm, reflecting POE micelle size. In panel B, colloid from RTN/HPMCAS-L was always larger than from RTN/PVP-VA.

Table 4. The observed and fitted permeation coefficient (P_{app}), k_p, flux (J_s) and the permeated amount of RTN solution and RTN tablets (Mean±SD, n=3)

	Permeation Coefficient (P_{app})(cm/sec) x10^6	Kp' (sec^{-1}) x10^6	Fitted Permeation Coefficient (P_{app})(cm/sec) x10^6	Kp' from fitted P_{app} (sec^{-1}) x10^6	Flux (Js) (μg min^{-1} cm^{-2})	Permeated amount % (at the end of 360 min)
Solution	9.30±1.83	1.19±0.2394	7.645±1.52*	0.977±0.195*	0.00100±0.00020	2.32±0.003
HPMCAS-L tablet	3.90±0.30	0.498±3.85	4.04±1.02**	0.517±0.106**	0.000430±0.000034	1.03±0.05
PVP-VA tablet	10.2±0.60	1.30±7.71	8.64±1.84**	1.10±0.92**	0.0618±0.0065	2.20±0.02
NORVIR tablet	14.7±8.46	1.88±1.09	8.72±4.60**	1.11±0.48**	0.00160+0.00090	2.02±0.64

* The equation of $M_b = M_0 - M_0 * e^{-kp't}$ (Figure 2) was used to fit the P_{app} values of solution from HFM. The fitted P_{app} was obtained via Solver.

**The fitted P_{app} for tablets were calculated via Eq.9 and Solver by using the k_d from tablet 'dissolution only' (0.398±0.0027 min^{-1} for HPMCAS-L; 0.0374±0.0010 min^{-1} for PVP-VA; 0.0239±0.0039 min^{-1} for Norvir Tablet) and kp' from the fitted P_{app} value (7.649 x10^{-6} cm/sec) of solution from HFM. For conversion of k_p' and P_{app}, Eq.8 was used.

Figure 12 plots the fitted and observed D-HFM permeation profile of solution and the predicted and observed D-HFM permeation profile of RTN tablets. The receiver mass values through HFM from tablets were predicted using the k_d from tablet 'dissolution only' study (0.398±0.0027 min^{-1} for HPMCAS-L; 0.0374±0.0010 min^{-1} for PVP-VA; 0.0239±0.0039 min^{-1} for Norvir Tablet) and k_p' from the fitted P_{app} value (7.645 x10^{-6} cm/sec) of solution from HFM. The predicted profile, which employed the higher P_{app} value from the solution formulation (i.e. from RTN/PVP-VA formulation), was about twice as high as the observed tablet profile (i.e. from RTN/HPMCAS-L formulation) and almost same from PVP-VA tablet and Norvir tablet. Results reflect the apparent P_{app} difference from the two different ASDs. While the fitted drug P_{app} value of solution was 7.645 x10^{-6} cm/sec, it was 4.043 x10^{-6} cm/sec, 8.637 x10^{-6} cm/sec, 8.721 x10^{-6} cm/sec for HPMCAS-L, PVP-VA and Norvir tablet (Table 4). By using these fitted P_{app} values, the fitted mass of RTN through HFM from tablets were also calculated. Fitted and observed receiver mass values through HFM from tablets were given in Figure S4.

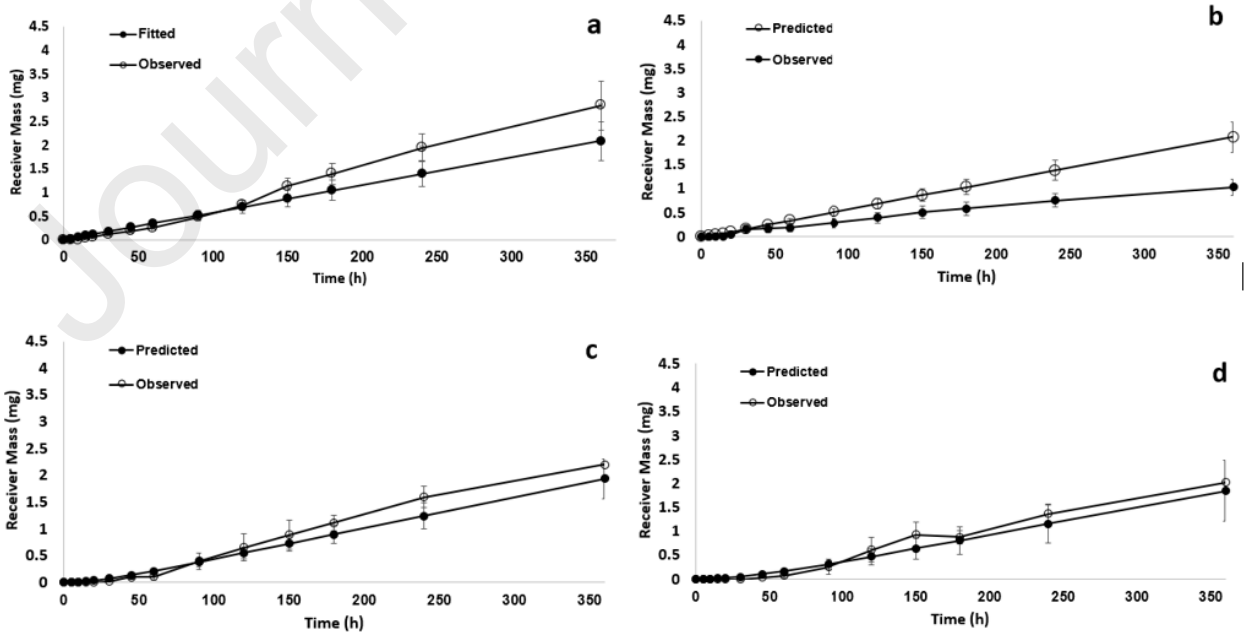

Figure 12. Fitted and observed receiver mass values through HFM from solution (panel a), predicted and observed receiver mass values through HFM from HPMCAS-L tablet (panel b), from PVP-VA (panel c) and from Norvir tablet (panel d).

4.CONCLUSION

This study provides a comprehensive evaluation of the effects of formulation and process parameters on the critical quality attributes and the dissolution/permeation performance of tablets containing HPMCAS-L SDDs. Tablets containing RTN SDD powders with HPMCAS-L were successfully prepared and optimized. Formulation parameters were optimized via experimental design. SDD powder prepared with 70 °C of inlet temperature, 65.5% of the amount of the SDD powder and 10% of the disintegrant level were identified as optimal via 3D surface graphs, with acceptable hardness and favorable disintegration. With these parameters, tablets were prepared with either MCC or DCP filler, and with CCS, CP or SSG disintegrants, and dissolution profiles were evaluated. The tablets containing MCC and CCS exhibited best dissolution profiles, such that optimal tablet formulation parameters were: SDD powder prepared with 70 °C of inlet temperature, 65.5% (w/w) tablet as SDD powder level, 24% (w/w) of MCC as a filler, 10% (w/w) of CCS as a disintegrant, and 0.5% (w/w) of MgS as a lubricant. To optimize tableting, 1, 2, 4, 7, 14, and 17 kN compaction forces were applied for direct compression, and 1, 2, 4,7, 12 and 17 kN compaction were applied to granules (prepared with 14 kN pre-compaction force) for dry granulation method. In all cases, the porosity % and Heckel in die values were lower for direct compression than for dry granulation. Oppositely, tensile strength was higher for direct compression than for dry granulation. The highest dissolution profiles and acceptable hardness properties were obtained via dry granulation using 14kN (pre-compaction force)+7kN of compaction force. Also, tablets using these formulation and process parameters, but where SDD was prepared using 140 °C inlet temperature were made; however, RTN melted, causing bridging and lower dissolution.

These optimum tablet parameters from HPMCAS-L were applied to the PVP-VA, HPMCAS L:H and SoluPlus ASDs. Dissolution (only) and D-HFM dissolution/permeation profiles were compared to those of HPMCAS-L and Norvir tablet. While the % permeated amount of RTN from HPMCAS-L tablet was 1% after 360 min, it was about 2 % from PVP-VA-based tablet, which was similar to solution and Norvir® tablet. These results may reflect the dissolution-resulting colloid as a critical component to overall drug absorption from ASD, beyond even favorable dissolution.

ACKNOWLEDGEMENT

This research was supported by the Scientific and Technological Research Council of Turkey (BIDEB 2219 (Project code: 1059B192000617).

DECLARATION OF COMPETITION INTEREST

The authors declare that they have no known competing financial interests or personal relationships that could have appeared to influence the work reported in this paper.

APPENDIX A. SUPPLEMENTARY MATERIAL

Supplementary material to this article can be found online.

REFERENCES

Adeleye, O.A., 2019. Relationship between compression pressure, mechanical strength and release properties of tablets. Polim. Med 49, 27-33.

Adhikari, A., Polli, J.E., 2020. Characterization of grades of HPMCAS spray dried dispersions of itraconazole based on supersaturation kinetics and molecular interactions impacting formulation performance. Pharmaceutical research 37, 1-15.

Adhikari, A., Seo, P.R., Polli, J.E., 2022a. Characterization of dissolution-permeation system using hollow fiber membrane module and utility to predict in vivo drug permeation across BCS classes. Journal of Pharmaceutical Sciences 111, 3075-3087.

Adhikari, A., Seo, P.R., Polli, J.E., 2022b. Dissolution-Hollow Fiber Membrane (D-HFM) system to anticipate biopharmaceutics risk of tablets and capsules. Journal of Pharmaceutical Sciences.

Aguiar, A., Wheeler, L., Fusari, S., Zelmer, J., 1968. Evaluation of physical and pharmaceutical factors involved in drug release and availability from chloramphenicol capsules. Journal of Pharmaceutical Sciences 57, 1844-1850.

Al-Ibraheemi, Z.A.M., Anuar, M., Taip, F., Amin, M., Tahir, S., Mahdi, A.B., 2013. Deformation and mechanical characteristics of compacted binary mixtures of plastic (microcrystalline cellulose), elastic (sodium starch glycolate), and brittle (lactose monohydrate) pharmaceutical excipients. Particulate Science and Technology 31, 561-567.

Alonzo, D.E., Zhang, G.G., Zhou, D., Gao, Y., Taylor, L.S., 2010. Understanding the behavior of amorphous pharmaceutical systems during dissolution. Pharmaceutical research 27, 608-618.

Ariyasu, A., Hattori, Y., Otsuka, M., 2016. Delay effect of magnesium stearate on tablet dissolution in acidic medium. International journal of pharmaceutics 511, 757-764.

Arshad, M.S., Zafar, S., Yousef, B., Alyassin, Y., Ali, R., AlAsiri, A., Chang, M.-W., Ahmad, Z., Elkordy, A.A., Faheem, A., 2021. A review of emerging technologies enabling improved solid oral dosage form manufacturing and processing. Advanced drug delivery reviews 178, 113840.

Ayenew, Z., Paudel, A., Van den Mooter, G., 2012. Can compression induce demixing in amorphous solid dispersions? A case study of naproxen–PVP K25. European Journal of Pharmaceutics and Biopharmaceutics 81, 207-213.

Bauhuber, S., Warnke, G., Berardi, A., 2021. Disintegrant selection in hydrophobic tablet formulations. Journal of Pharmaceutical Sciences 110, 2028-2037.

Berkenkemper, S., Kleinebudde, P., 2022. Compressibility analysis as robust in-die compression analysis for describing tableting behaviour. RPS Pharmacy and Pharmacology Reports 1, rqac004.

Bhujbal, S.V., Mitra, B., Jain, U., Gong, Y., Agrawal, A., Karki, S., Taylor, L.S., Kumar, S., Zhou, Q.T., 2021. Pharmaceutical amorphous solid dispersion: A review of manufacturing strategies. Acta Pharmaceutica Sinica B 11, 2505-2536.

Chakravarty, P., Lubach, J.W., Hau, J., Nagapudi, K., 2017. A rational approach towards development of amorphous solid dispersions: experimental and computational techniques. International Journal of Pharmaceutics 519, 44-57.

Corrie, L., Ajjarapu, S., Banda, S., Parvathaneni, M., Bolla, P.K., Kommineni, N., 2023. HPMCAS-based amorphous solid dispersions in clinic: a review on manufacturing techniques (hot melt extrusion and spray drying), marketed products and patents. Materials 16, 6616.

Demina, N., Bobkova, N., Solodun, E., Anurova, M., Bakhrushina, E., Krasnyuk, I., 2018. Influence of Various Disintegrants on the Quality of Microcrystalline Cellulose Tablets. Pharmaceutical Chemistry Journal 52, 781-785.

Démuth, B., Nagy, Z.K., Balogh, A., Vigh, T., Marosi, G., Verreck, G., Van Assche, I., Brewster, M., 2015. Downstream processing of polymer-based amorphous solid dispersions to generate tablet formulations. International journal of pharmaceutics 486, 268-286.

Dhumal, G., Treffer, D., Polli, J.E., 2024. Concordance of vacuum compression molding with spray drying in screening of amorphous solid dispersions of itraconazole. International Journal of Pharmaceutics 654, 123952.

DiNunzio, J.C., Miller, D.A., Yang, W., McGinity, J.W., Williams III, R.O., 2008. Amorphous compositions using concentration enhancing polymers for improved bioavailability of itraconazole. Molecular pharmaceutics 5, 968-980.

DiNunzio, J.C., Schilling, S.U., Coney, A.W., Hughey, J.R., Kaneko, N., McGinity, J.W., 2012. Use of highly compressible Ceolus™ microcrystalline cellulose for improved dosage form properties containing a hydrophilic solid dispersion. Drug Development and Industrial Pharmacy 38, 180-189.

Duddu, S.P., Sokoloski, T.D., 1995. Dielectric Analysis in the Characterization of Amorphous Pharmaceutical Solids. 1. Molecular Mobility in Poly (vinylpyrro1idone)-Water Systems in the Glassy State. Journal of pharmaceutical sciences 84, 773-776.

Dulla, O., Sultana, S., Shohag Hosen, M., 2018. In vitro comparative quality evaluation of different brands of esomeprazole tablets available in selected community pharmacies in Dhaka, Bangladesh. BMC research notes 11, 1-5.

Ekdahl, A., Mudie, D., Malewski, D., Amidon, G., Goodwin, A., 2019. Effect of spray-dried particle morphology on mechanical and flow properties of felodipine in PVP VA amorphous solid dispersions. Journal of pharmaceutical sciences 108, 3657-3666.

Ellenberger, D.J., Miller, D.A., Kucera, S.U., Williams III, R.O., 2018. Generation of a weakly acidic amorphous solid dispersion of the weak base ritonavir with equivalent in vitro and in vivo performance to Norvir tablet. AAPS PharmSciTech 19, 1985-1997.

Elsergany, R.N., Vreeman, G., Sun, C.C., 2023. An approach for predicting the true density of powders based on in-die compression data. International journal of pharmaceutics 637, 122875.

Fakes, M.G., Vakkalagadda, B.J., Qian, F., Desikan, S., Gandhi, R.B., Lai, C., Hsieh, A., Franchini, M.K., Toale, H., Brown, J., 2009. Enhancement of oral bioavailability of an HIV-attachment inhibitor by nanosizing and amorphous formulation approaches. International journal of pharmaceutics 370, 167-174.

Faroongsarng, D., Peck, G.E., 1994. The swelling & water uptake of tablets III: moisture sorption behavior of tablet disintegrants. Drug development and industrial pharmacy 20, 779-798.

Friesen, D.T., Shanker, R., Crew, M., Smithey, D.T., Curatolo, W., Nightingale, J., 2008. Hydroxypropyl methylcellulose acetate succinate-based spray-dried dispersions: an overview. Molecular pharmaceutics 5, 1003-1019.

Hancock, B.C., Zografi, G., 1994. The relationship between the glass transition temperature and the water content of amorphous pharmaceutical solids. Pharmaceutical research 11, 471-477.

Heckel, R., 1961. Density-pressure relationships in powder compaction. Trans. Metal. Soc. AIME 221, 671-675.

Honick, M., Das, S., Hoag, S.W., Muller, F.X., Alayoubi, A., Feng, X., Zidan, A., Ashraf, M., Polli, J.E., 2020a. The effects of spray drying, HPMCAS grade, and compression speed on the compaction properties of itraconazole-HPMCAS spray dried dispersions. European Journal of Pharmaceutical Sciences 155, 105556.

Honick, M., Das, S., Hoag, S.W., Muller, F.X., Alayoubi, A., Feng, X., Zidan, A., Ashraf, M., Polli, J.E., 2020b. The effects of spray drying, HPMCAS grade, and compression speed on the compaction properties of itraconazole-HPMCAS spray dried dispersions. Eur J Pharm Sci 155, 105556.

Indulkar, A.S., Lou, X., Zhang, G.G., Taylor, L.S., 2019. Insights into the dissolution mechanism of ritonavir–copovidone amorphous solid dispersions: importance of congruent release for enhanced performance. Molecular pharmaceutics 16, 1327-1339.

Iwao, Y., Tanaka, S., Uchimoto, T., Noguchi, S., Itai, S., 2013. An easy-to-use approach for determining the disintegration ability of disintegrants by analysis of available surface area. International journal of pharmaceutics 448, 1-8.

Iyer, R., Hegde, S., Zhang, Y.-E., Dinunzio, J., Singhal, D., Malick, A., Amidon, G., 2013. The impact of hot melt extrusion and spray drying on mechanical properties and tableting indices of materials used in pharmaceutical development. Journal of pharmaceutical sciences 102, 3604-3613.

JRSPharma, 2020. Manufacturer website. https://www.jrspharma.com/pharma_en/, accessed 29 Dec 2024.

Karakucuk, A., Celebi, N., Teksin, Z.S., 2016. Preparation of ritonavir nanosuspensions by microfluidization using polymeric stabilizers: I. A Design of Experiment approach. European Journal of Pharmaceutical Sciences 95, 111-121.

Karakucuk, A., Teksin, Z.S., Eroglu, H., Celebi, N., 2019. Evaluation of improved oral bioavailability of ritonavir nanosuspension. European Journal of Pharmaceutical Sciences 131, 153-158.

Karmakar, P., Kibria, M.G., 2012. In-vitro comparative evaluation of quality control parameters between paracetamol and paracetamol/caffeine tablets available in Bangladesh. International Current Pharmaceutical Journal 1, 103-109.

Khan, K., Musikabhumma, P., 1981. Effect of slugging pressure on the properties of granules and tablets prepared from potassium phenethicillin. Journal of Pharmacy and Pharmacology 33, 627-631.

Markl, D., Zeitler, J.A., 2017. A review of disintegration mechanisms and measurement techniques. Pharmaceutical research 34, 890-917.

Men, S., Polli, J.E., 2024. Microscope-enabled disc dissolution system: Concordance between drug and polymer dissolution from an amorphous solid dispersion disc and visual disc degradation. Journal of Pharmaceutical Sciences 113, 3586-3598.

Monographs, O., 2009a. United States Pharmacopeia-National Formulary (USP 29-NF 24)p.2778, Rockville, Maryland: United States Pharmacopeial Convention Inc, p. 2778.

Monographs, O., 2009b. United States Pharmacopeia-National Formulary (USP 32-NF 27) p.726, Rockville, Maryland: United States Pharmacopeial Convention Inc, p. 726.

Moseson, D.E., Tran, T.B., Karunakaran, B., Ambardekar, R., Hiew, T.N., 2024. Trends in amorphous solid dispersion drug products approved by the US Food and Drug Administration between 2012 and 2023. International journal of pharmaceutics: X 7, 100259.

Nunes, P.D., Ferreira, A.F., Pinto, J.F., Bauer-Brandl, A., Brandl, M., Henriques, J., Paiva, A.M., 2023. In vitro dissolution/permeation tools for amorphous solid dispersions bioavailability forecasting II: Comparison and mechanistic insights. European Journal of Pharmaceutical Sciences 188, 106513.

Ogawa, N., Hiramatsu, T., Suzuki, R., Okamoto, R., Shibagaki, K., Fujita, K., Takahashi, C., Kawashima, Y., Yamamoto, H., 2018. Improvement in the water solubility of drugs with a solid dispersion system by spray drying and hot-melt extrusion with using the amphiphilic polyvinyl caprolactam-polyvinyl acetate-polyethylene glycol graft copolymer and d-mannitol. European Journal of Pharmaceutical Sciences 111, 205-214.

Oktay, A.N., Polli, J.E., 2024. Screening of Polymers for Oral Ritonavir Amorphous Solid Dispersions by Film Casting. Pharmaceutics 16, 1373.

Omar, C.S., Dhenge, R.M., Osborne, J.D., Althaus, T.O., Palzer, S., Hounslow, M.J., Salman, A.D., 2015. Roller compaction: Effect of morphology and amorphous content of lactose powder on product quality. International journal of pharmaceutics 496, 63-74.

Pan, S., Sharma, P.K., Malviya, R., 2015. Evaluation of Compression Force on the Dissolution Profile of Paracetamol Tablets. Middle-East Journal of Scientific Research 23, 1020-1022.

Pandi, P., Bulusu, R., Kommineni, N., Khan, W., Singh, M., 2020. Amorphous solid dispersions: An update for preparation, characterization, mechanism on bioavailability, stability, regulatory considerations and marketed products. International journal of pharmaceutics 586, 119560.

Patel, R.P., Taylor, L.S., Polli, J.E., 2025. Impact of drug incorporation into micelle on reduced griseofulvin and meloxicam permeation across a hollow fiber membrane. Journal of Pharmaceutical Sciences 114, 402-415.

Polli, J.E., 2022. A Simple One-Parameter Percent Dissolved Versus Time Dissolution Equation that Accommodates Sink and Non-sink Conditions via Drug Solubility and Dissolution Volume. The AAPS journal 25, 1.

Polli, J.E., Rekhi, G.S., Augsburger, L.L., Shah, V.P., 1997. Methods to compare dissolution profiles and a rationale for wide dissolution specifications for metoprolol tartrate tablets. Journal of Pharmaceutical Sciences 86, 690-700.

Purohit, H.S., Taylor, L.S., 2017. Phase behavior of ritonavir amorphous solid dispersions during hydration and dissolution. Pharmaceutical research 34, 2842-2861.

Rosenberg, J., Reinhold, U., Liepold, B., Berndl, G., Breitenbach, J., Alani, L., Ghosh, S., 2012. Solid pharmaceutical dosage form. Google Patents.

Sagiraju, S.R., Aldeniz, E., Ekmeksi, E., Dude, U., DemİRay, B., 2024. The Effect Of Compaction Force On Tablet Hardness And Dissolution Rate Of A Poorly Soluble, BCS Class II, Micronized API In Lactose-Based Immediate Release Formulations: A Case Study With RSM Historical Data Review Using Design Of Experiment. 2, 776-786.

Sauer, A., Warashina, S., Mishra, S.M., Lesser, I., Kirchhoefer, K., 2021. Downstream processing of spray-dried ASD with hypromellose acetate succinate–Roller compaction and subsequent compression into high ASD load tablets. International Journal of Pharmaceutics: X 3, 100099.

Seo, P.R., Shah, V.P., Polli, J.E., 2002. Novel metrics to compare dissolution profiles. Pharmaceutical development and technology 7, 257-265.

Shetty, N., Hau, J., Tang, S., Chiang, P.-C., Liu, J., Jia, W., Lubach, J.W., Nagapudi, K., Hou, H.H., 2025. Assessing the impacts of drug loading and polymer type on dissolution behavior and diffusive flux of GDC-6893 amorphous solid dispersions. Journal of Pharmaceutical Sciences 114, 103686.

Simões, M.F., Pinto, R.M., Simões, S., 2019. Hot-melt extrusion in the pharmaceutical industry: toward filing a new drug application. Drug Discovery Today 24, 1749-1768.

Singh, A., Van den Mooter, G., 2016. Spray drying formulation of amorphous solid dispersions. Advanced drug delivery reviews 100, 27-50.

Stewart, A.M., Grass, M.E., Brodeur, T.J., Goodwin, A.K., Morgen, M.M., Friesen, D.T., Vodak, D.T., 2017. Impact of drug-rich colloids of itraconazole and HPMCAS on membrane flux in vitro and oral bioavailability in rats. Molecular pharmaceutics 14, 2437-2449.

Tao, Y., Tang, Z., Huang, Q., Xu, X., Cheng, X., Zhang, G., Jing, X., Li, X., Liang, J., Granato, D., 2024. Effects of spray drying temperature on physicochemical properties of grapeseed oil microcapsules and the encapsulation efficiency of pterostilbene. LWT 193, 115779.

United States Pharmacopeia, <701> Disintegration. https://www.usp.org/harmonization-standards/pdg/general-methods/disintegration, (accessed 01 January 2025)

United States Pharmacopeia, 2012. <1217>Tablet Breaking Force. The United States Pharmacopeia 35. https://www.drugfuture.com/Pharmacopoeia/usp35/PDF/0868-0870%20%5B1217%5D%20TABLET%20BREAKING%20FORCE.pdf, (accessed 25 February 2024).

Vaithianathan, S., Haidar, S.H., Zhang, X., Jiang, W., Avon, C., Dowling, T.C., Shao, C., Kane, M., Hoag, S.W., Flasar, M.H., 2016. Effect of common excipients on the oral drug absorption of biopharmaceutics classification system class 3 drugs cimetidine and acyclovir. Journal of pharmaceutical sciences 105, 996-1005.

Vaka, S.R.K., Bommana, M.M., Desai, D., Djordjevic, J., Phuapradit, W., Shah, N., 2014. Excipients for amorphous solid dispersions, Amorphous solid dispersions: Theory and practice. Springer, pp. 123-161.

Vehring, R., 2008. Pharmaceutical particle engineering via spray drying. Pharmaceutical research 25, 999-1022.

Walton, D., 2000. The morphology of spray-dried particles a qualitative view. Drying Technology 18, 1943-1986.

Wang, L.G., Omar, C., Litster, J.D., Li, J., Mitchell, N., Bellinghausen, S., Barrasso, D., Salman, A., Slade, D., 2021. Tableting model assessment of porosity and tensile strength using a continuous wet granulation route. International journal of pharmaceutics 607, 120934.

Yang, R., Mann, A.K., Van Duong, T., Ormes, J.D., Okoh, G.A., Hermans, A., Taylor, L.S., 2021. Drug release and nanodroplet formation from amorphous solid dispersions: insight into the roles of drug physicochemical properties and polymer selection. Molecular Pharmaceutics 18, 2066-2081.

Yu, D., Hoag, S.W., 2024. The impact of diluents on the compaction, dissolution, and physical stability of amorphous solid dispersion tablets. International Journal of Pharmaceutics 654, 123924.

Yu, D., Nie, H., Hoag, S.W., 2024. Comprehensive evaluation of polymer types and ratios in Spray-Dried Dispersions: Compaction, Dissolution, and physical stability. International Journal of Pharmaceutics 650, 123674.

Zarmpi, P., Flanagan, T., Meehan, E., Mann, J., Fotaki, N., 2020. Impact of magnesium stearate presence and variability on drug apparent solubility based on drug physicochemical properties. The AAPS journal 22, 75.

Zhang, W., Thool, P., Weitz, B.W., Hou, H.H., 2024. Investigating the effects of formulation variables on the disintegration of spray dried amorphous solid dispersion tablets. Journal of Pharmaceutical Sciences.

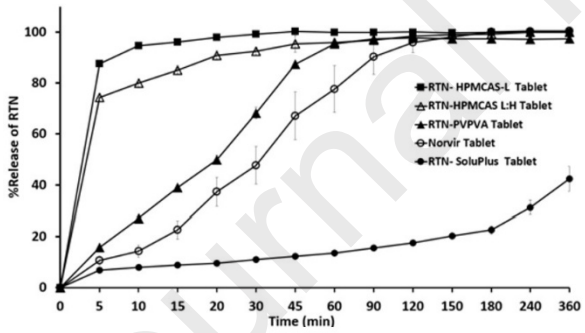

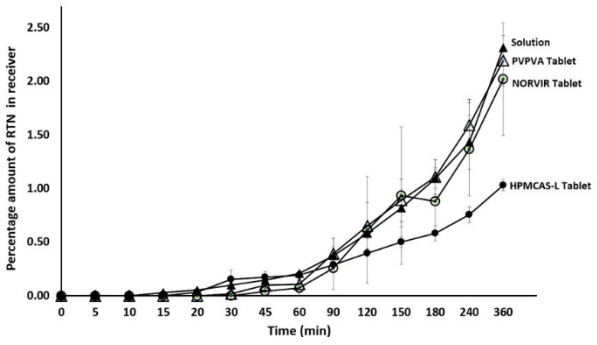

Declaration of interests

☐ The authors declare that they have no known competing financial interests or personal relationships that could have appeared to influence the work reported in this paper.

☒ The authors declare the following financial interests/personal relationships which may be considered as potential competing interests:

Ayse Nur OKTAY reports financial support was provided by The Scientific and Technological Research Council of Turkey.

Figure Captions

Figure 1. Scope and sequence of tablet formulation studies.

Figure 2. Scope and sequence of in vitro dissolution/permeation studies, after study 4 of tablet formulation studies.

Figure 3. 3D surface graphs showing the effect of study 1 parameters of inlet temperature, SDD powder level, and disintegrant level on tablet thickness.

Figure 4. 3D surface graphs showing the effect of study 1 parameters of inlet temperature, SDD powder level, and disintegrant level on tablet hardness.

Figure 5. 3D surface graphs showing the effect of study 1 parameters of inlet temperature, SDD powder level, and disintegrant level on disintegration time.

Figure 6. Dissolution profiles from study 2, where filler type and disintegrant type were varied.

Figure 7. The representative plots of in die tablet porosity % (a), Heckel in die (b) and Tensile strength (b) versus mean compaction pressures (mPa), and tensile strength versus in die porosity% values of tablets (d). Data indicates mean±SEM (n=3)

Figure 8. Interplay of process method and compaction force on RTN dissolution. Inset plot shows dissolution for only the first 60 min.

Figure 9. Dissolution profiles of optimum tablets with various polymers compared to the Norvir® tablet.

Figure 10. D-HFM permeation profiles of RTN tablets with various polymers.

Figure 11. Dynamic light scattering results of in vitro powder dissolution of samples RTN/HPMCAS-L SDD and RTN/PVP-VA SDD.

Figure 12. Fitted and observed receiver mass values through HFM from solution (panel a), predicted and observed receiver mass values through HFM from HPMCAS-L tablet (panel b), from PVP-VA (panel c) and from Norvir tablet (panel d).

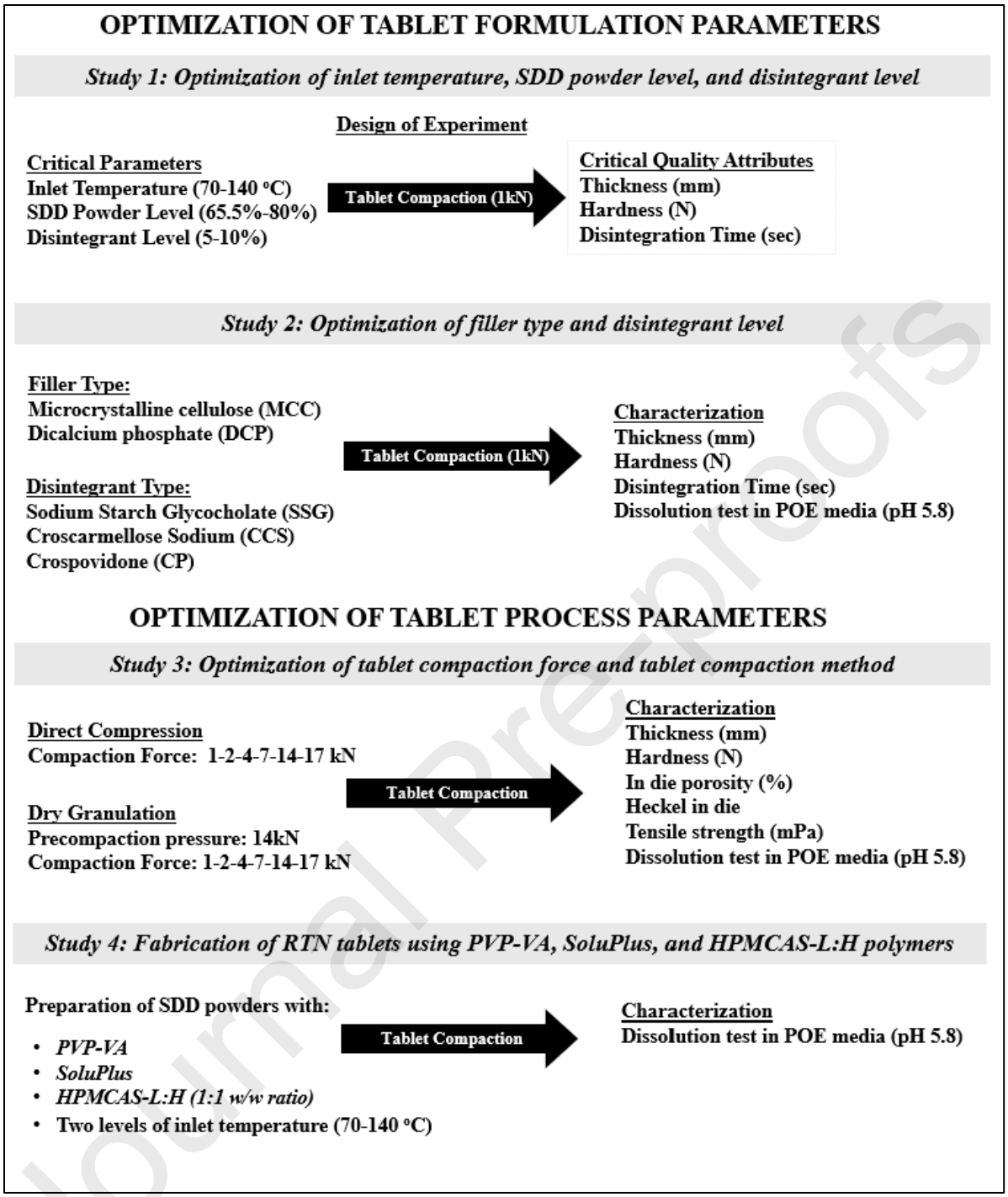

Figure 1. Scope and sequence of tablet formulation studies. Study 1 and study 2 focused on optimizing tablet formulation parameters, using HPMCAS-L. Study 3 focused on tablet process parameters, using HPMCAS-L. As results show, study 1 informed the use of lower SDD powder level (i.e. 65.5%), higher disintegrant level (i.e. 10%), and lower spray drier inlet temperature (i.e. 70°C) for subsequent study 2. Study 2 informed the use of MCC as filler and CCS as disintegrant in subsequent study 3. Study 3 identified the preference for dry granulation, including 14+7 kN compaction force. Study 4 applied these optimized process and formulation parameters to the fabrication of RTN tablets that used SDD from each PVP-VA, SoluPlus, and HPMCAS-L:H (1:1 w/w ratio). RTN tablets from HPMCAS-L and PVP-VA performed best and were subjected to subsequent in vitro dissolution/permeation evaluation.

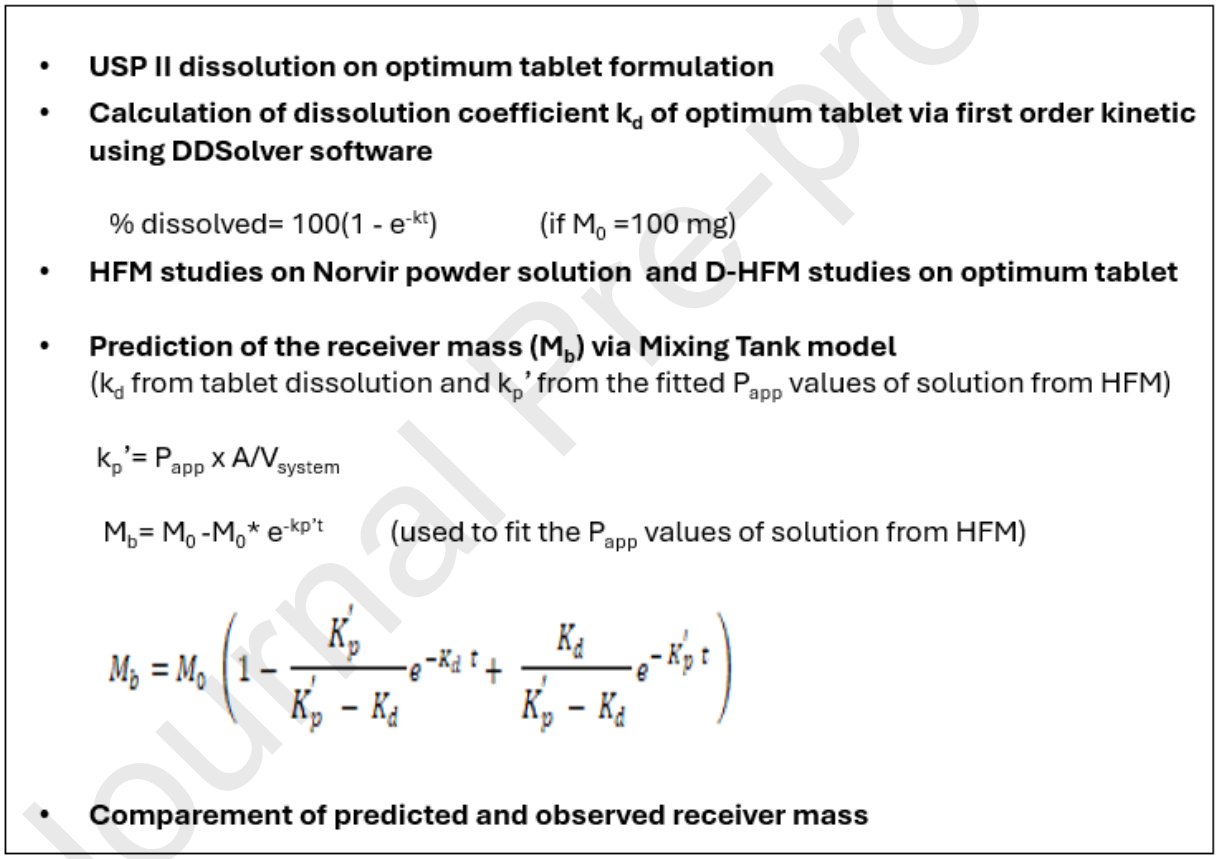

Figure 2. Scope and sequence of in vitro dissolution/permeation studies, after study 4 of tablet formulation studies. Dissolution/permeation studies used the D-HFM system. Also listed are USP II dissolution studies from the prior tablet formulation phase of studies, resulting in dissolution rate coefficient k_d. Tested formulations were tablet formulations that employed SDD from each HPMCAS-L and PVP-VA, along with commercial Norvir tablet. HFM permeation rate coefficient k_p was estimated from subjecting a solution fabricated from commercial Norvir powder to HFM permeation. For each of the two test tablets and Norvir tablets, predicted D-HFM absorption profiles were constructed from k_d and k_p, then compared to observed D-HFM absorption profiles.

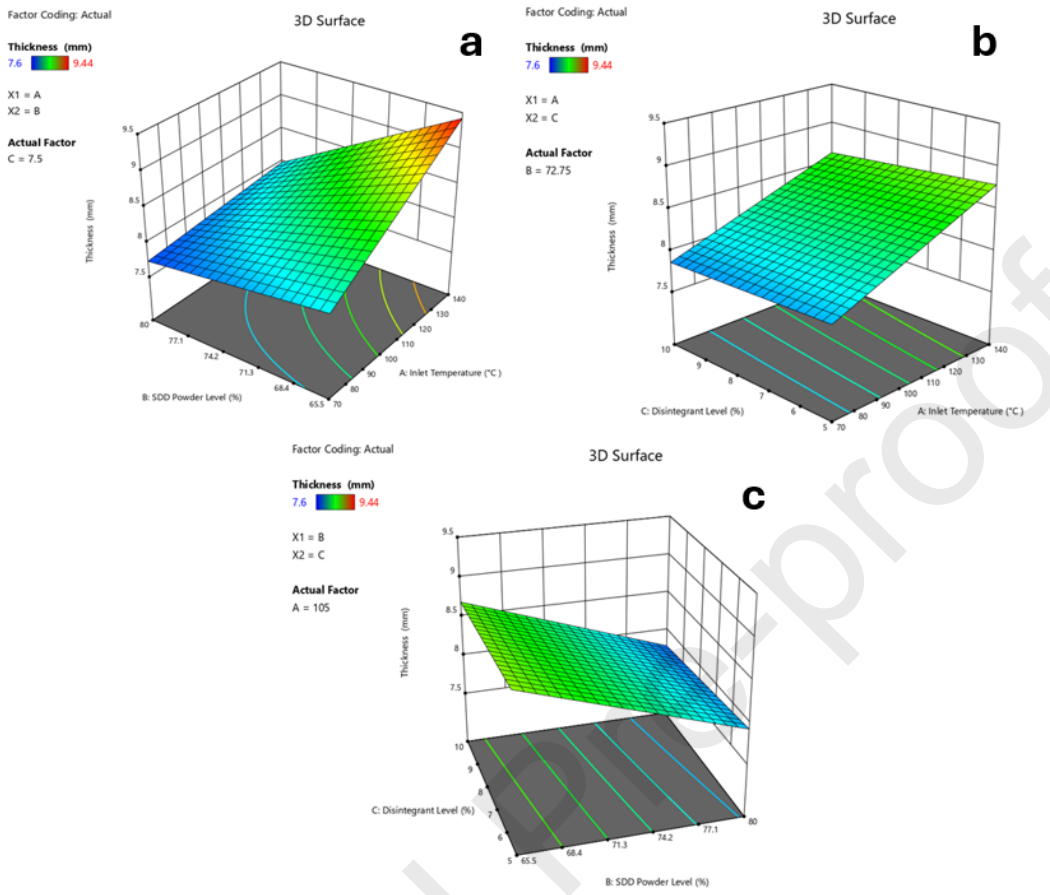

Figure 3. 3D surface graphs showing the effect of study 1 parameters of inlet temperature, SDD powder level, and disintegrant level on tablet thickness.

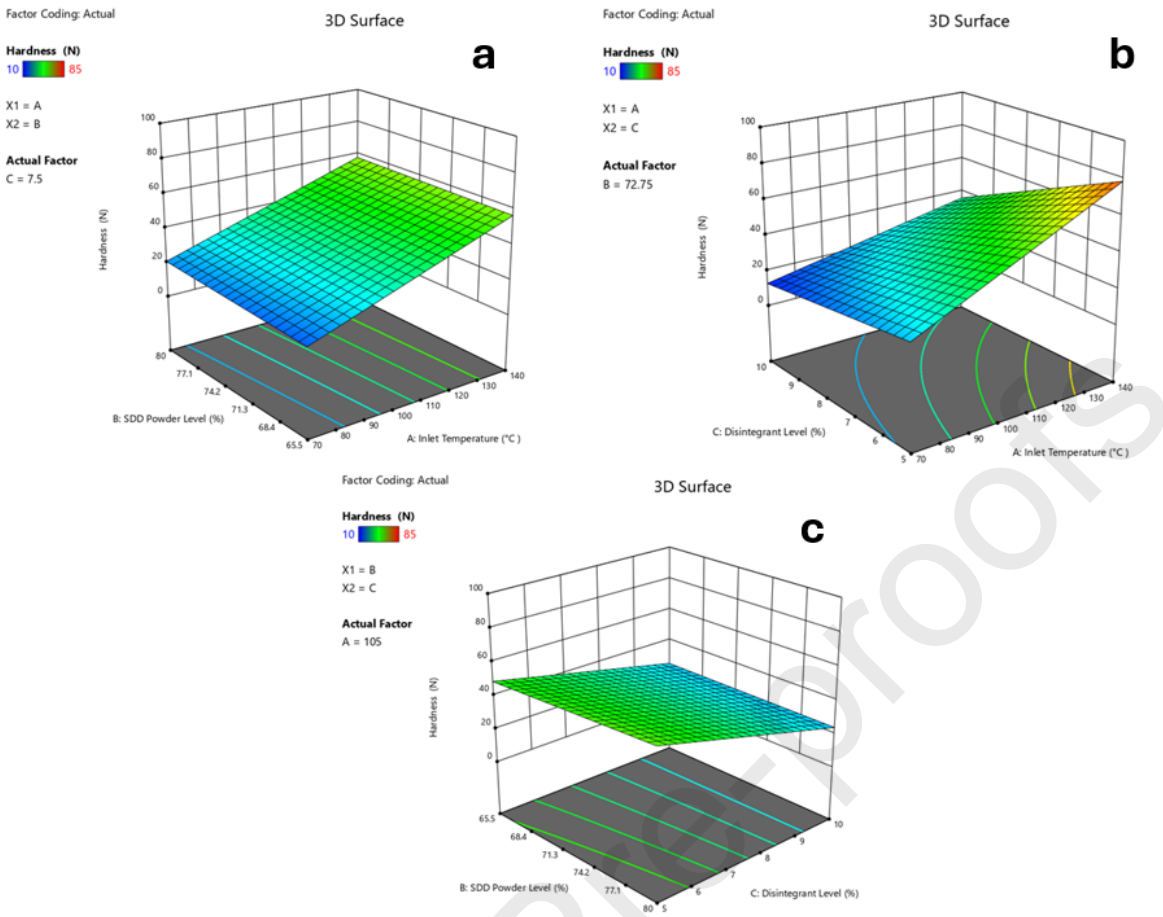

Figure 4. 3D surface graphs showing the effect of study 1 parameters of inlet temperature, SDD powder level, and disintegrant level on tablet hardness.

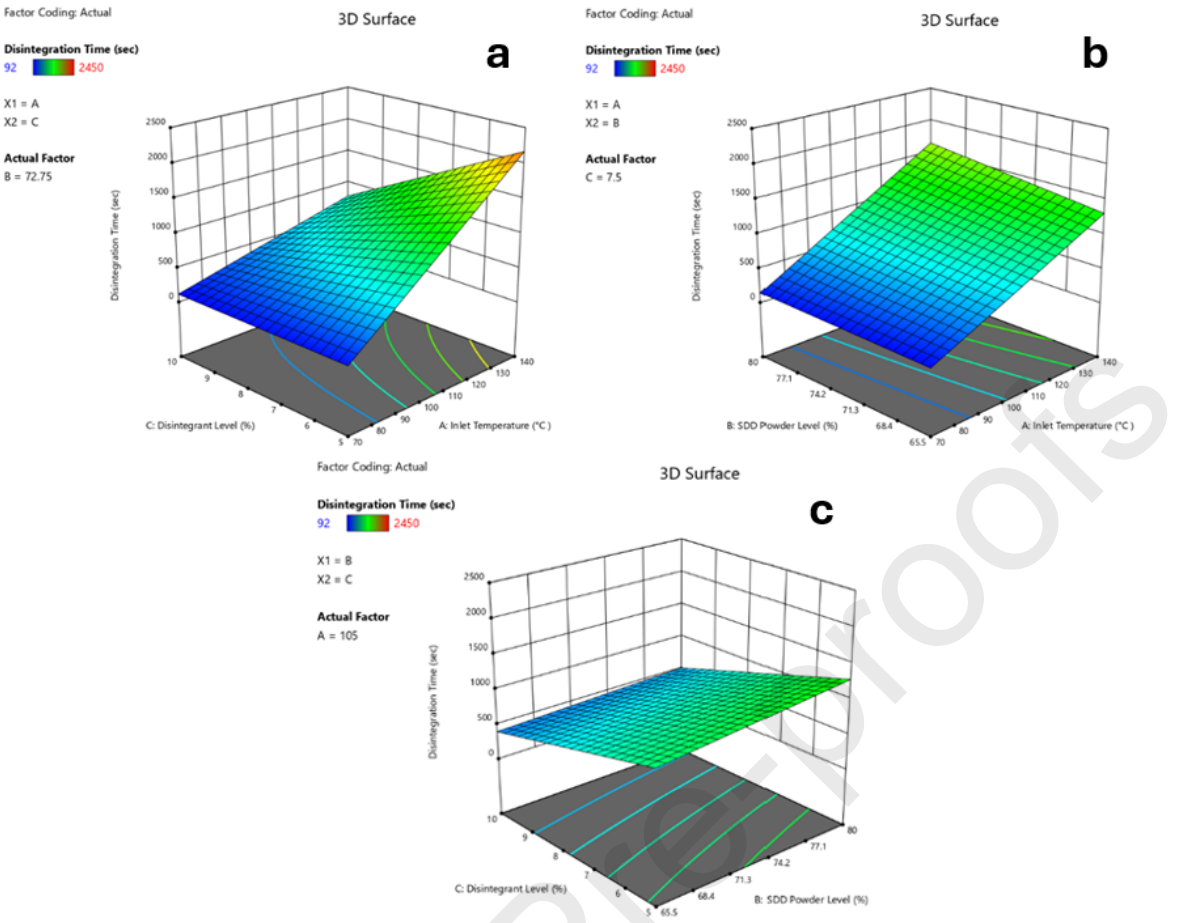

Figure 5. 3D surface graphs showing the effect of study 1 parameters of inlet temperature, SDD powder level, and disintegrant level on disintegration time.

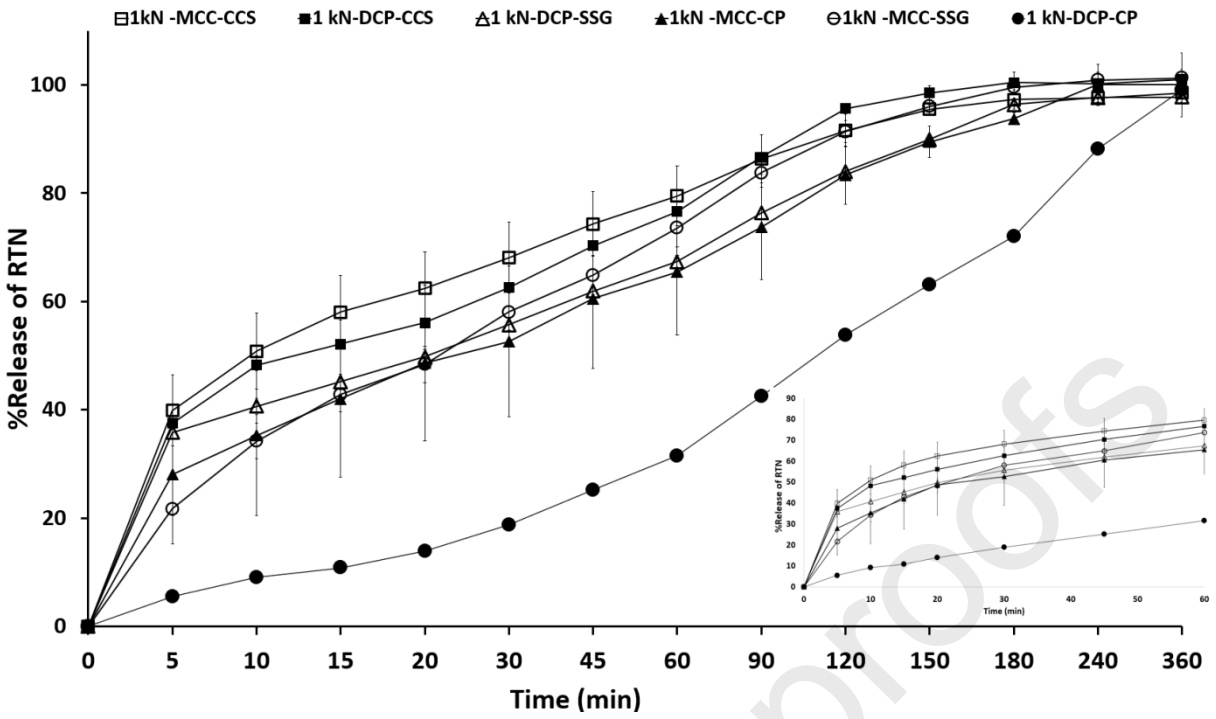

Figure 6. Dissolution profiles from study 2, where filler type and disintegrant type were varied. Fillers were MCC and DCP. Disintegrants were SSG, CCS, and CP.

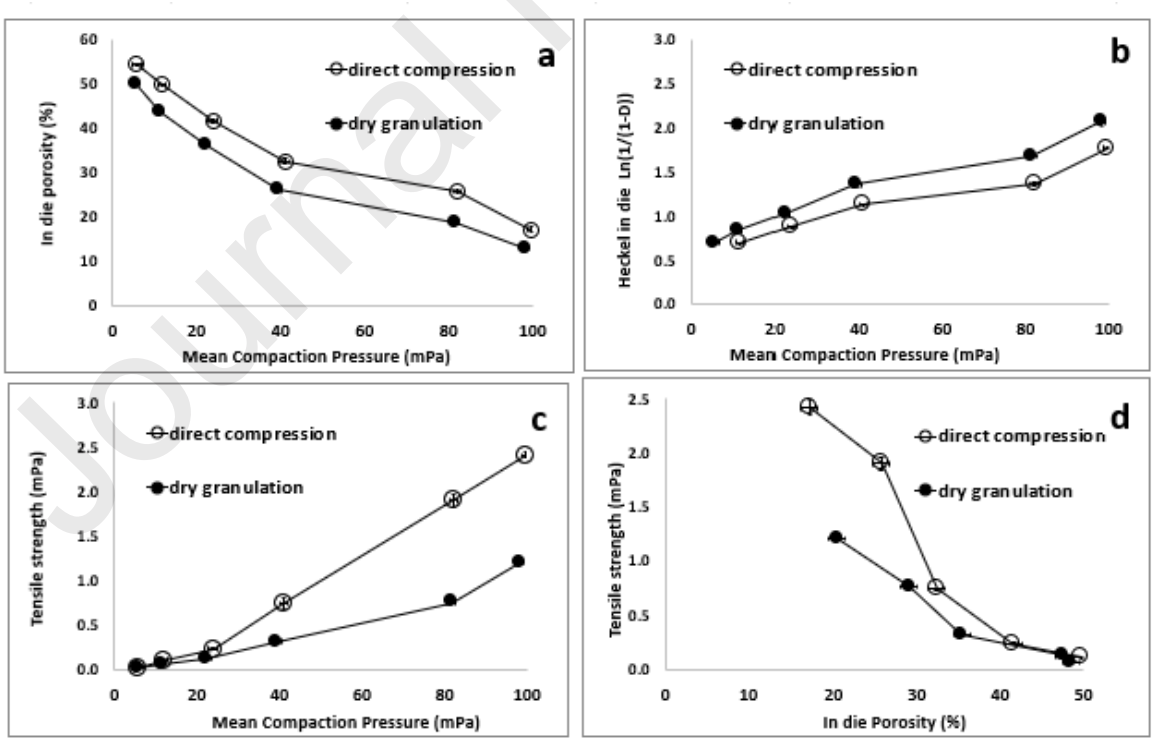

Figure 7. The representative plots of in die tablet porosity % (a), Heckel in die (b) and Tensile strength (b) versus mean compaction pressures (mPa), and tensile strength versus in die porosity% values of tablets (d). Data indicates mean±SEM (n=3)

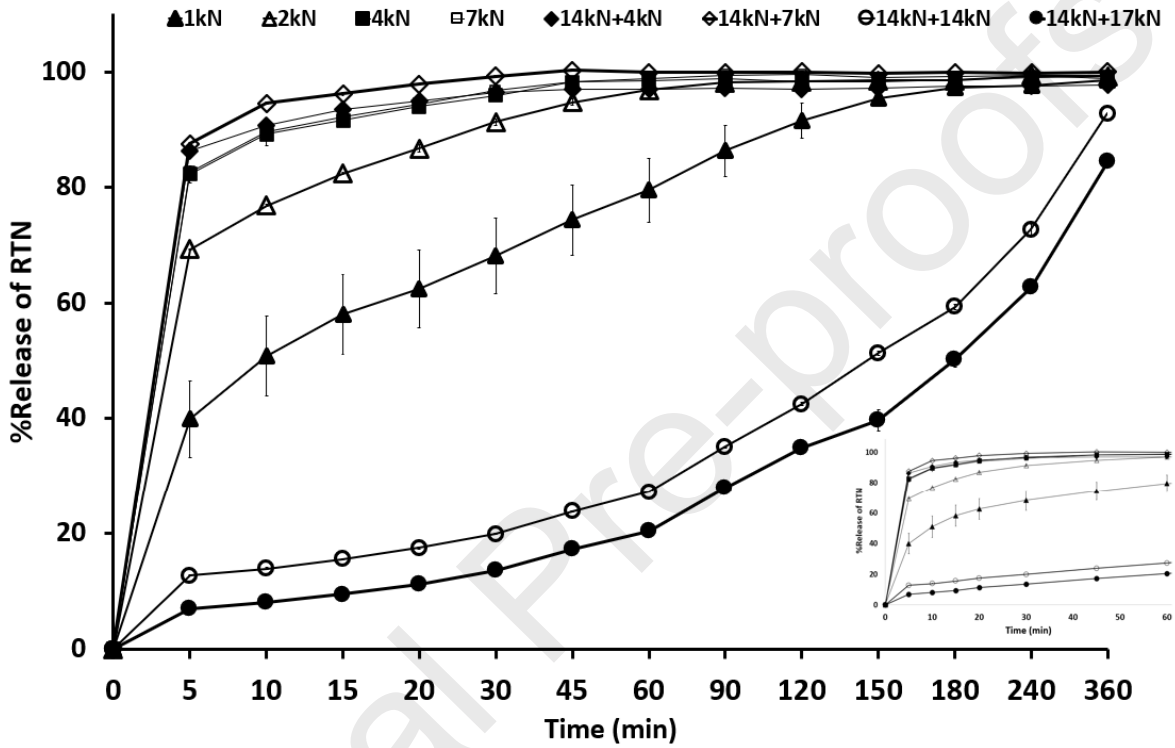

Figure 8. Interplay of process method and compaction force on RTN dissolution. Inset plot shows dissolution for only the first 60 min. Tablets were fabricated via both direct compression and dry granulation. In figure, the four formulations made via dry granulation include the pre-compression force of 14kN in label.

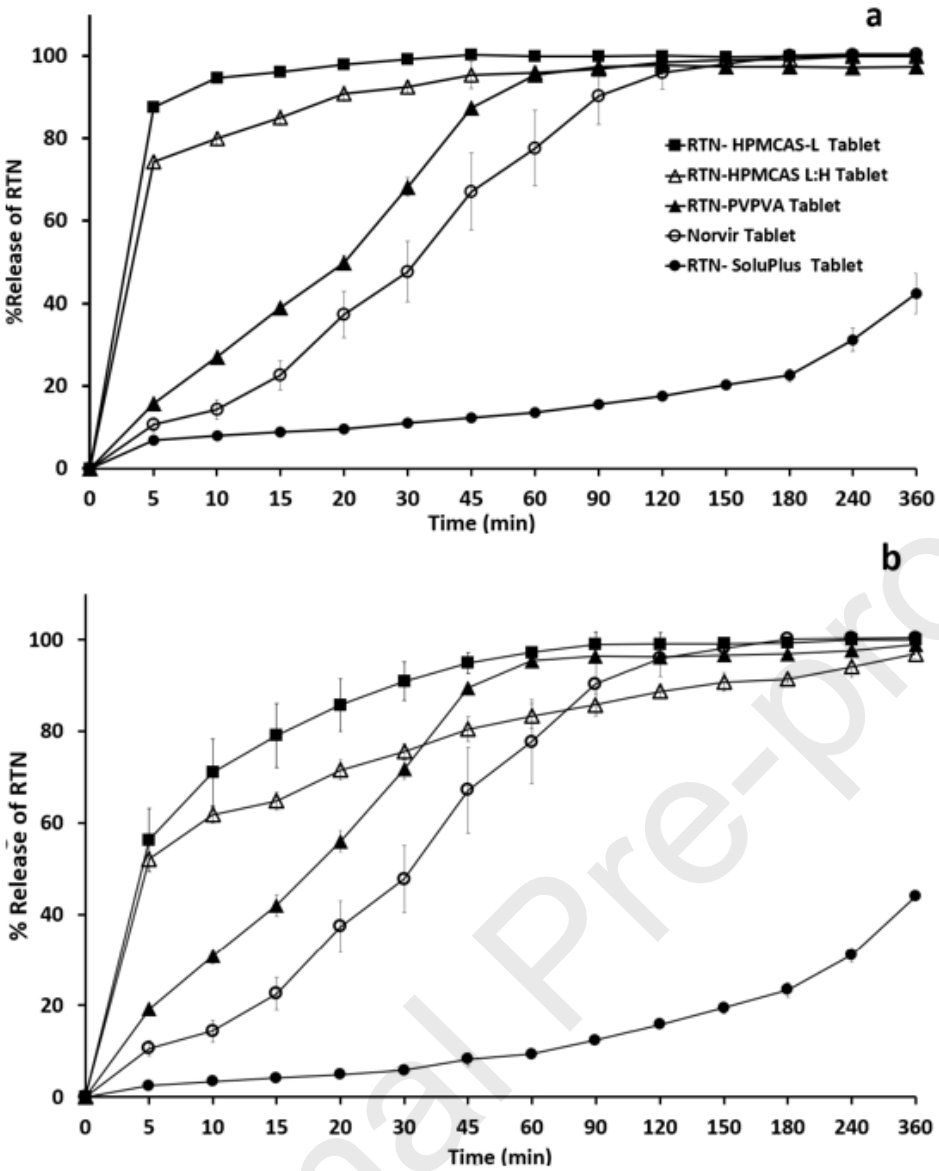

Figure 9. Dissolution profiles of optimum tablets with various polymers compared to the Norvir® tablet. Optimized tablets containing SDD fabricated using inlet temperature of 70°C (panel a), using inlet temperature of 140°C (panel b). The optimum RTN-HPMCAS-L tablet exhibited faster dissolution.

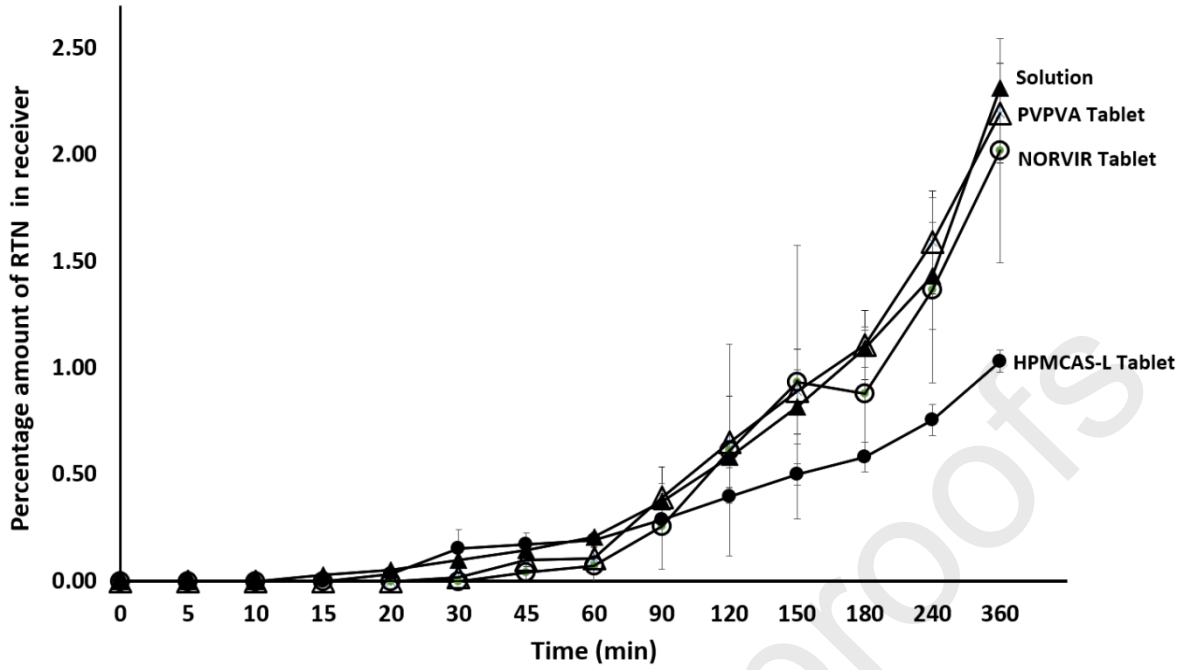

Figure 10. D-HFM permeation profiles of RTN tablets with various polymers. About 1% of drug dissolved and permeated from the HPMCAS-L tablet over 360 min. Also shown is RTN permeation profile from solution, where about 2% of drug permeated, similar to the PVP-VA polymer tablet and Norvir® tablet. Each tablet and solution contained 100 mg RTN.

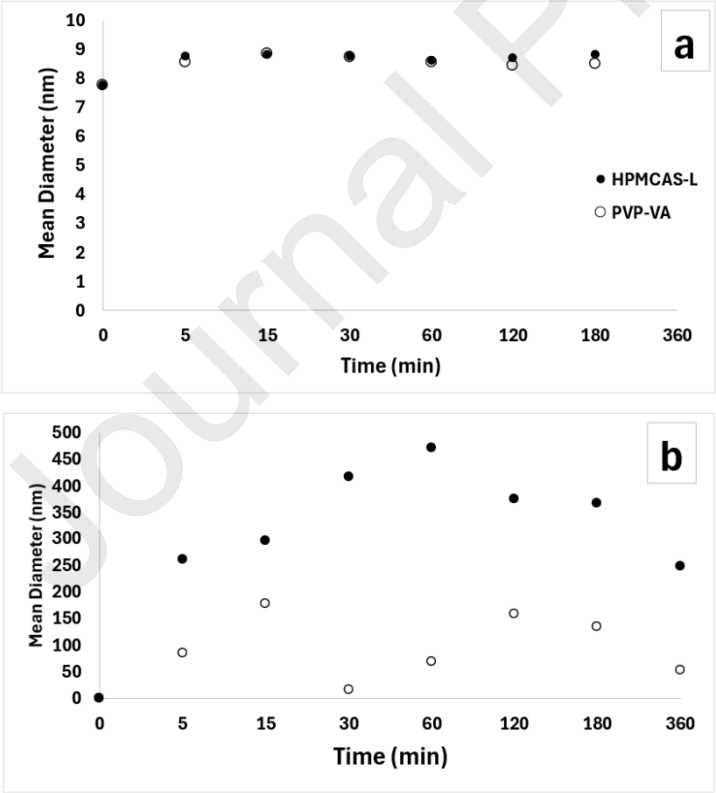

Figure 11. Dynamic light scattering results of in vitro powder dissolution of samples RTN/HPMCAS-L SDD and RTN/PVP-VA SDD. Dissolution media was maleic acid buffer (pH 5.8) with 60 mM POE in panel A, and without 60 mM POE in panel B. In panel A, colloid size

was always about 8nm, reflecting POE micelle size. In panel B, colloid from RTN/HPMCAS-L was always larger than from RTN/PVP-VA.

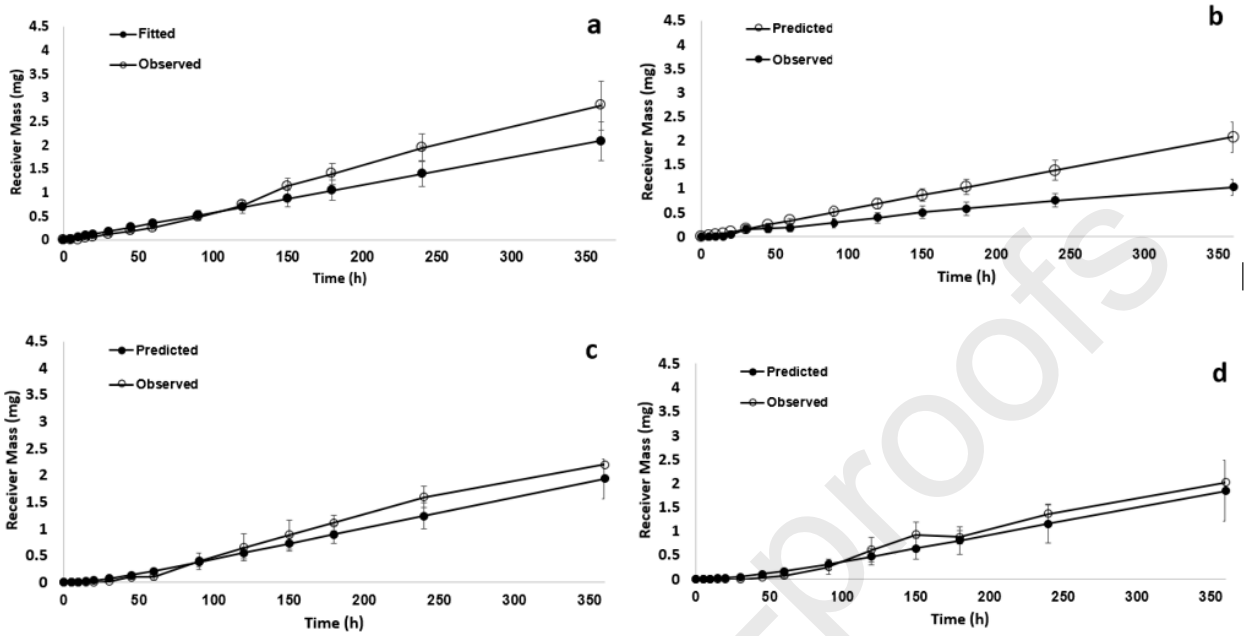

Figure 12. Fitted and observed receiver mass values through HFM from solution (panel a), predicted and observed receiver mass values through HFM from HPMCAS-L tablet (panel b), from PVP-VA (panel c) and from Norvir tablet (panel d).

Table Captions

Table 1. Tablet thickness, lengths, width, hardness and disintegration time from study 2.

Table 2. Tablet properties in study 3 using direct compression and dry granulation. Compaction force was varied.

Table 3. Effects of tablet compaction force on RTN tablet properties for direct compression and dry granulation.

Table 4. The observed and fitted permeation coefficient (P_{app}), k_p, flux (J_s) and the permeated amount of RTN solution and RTN tablets (Mean±SD, n=3)

Table 1. Tablet thickness, lengths, width, hardness and disintegration time from study 2. Formulations varied in fillers (MCC or DCP) and disintegrant (SSG, CCS, and CP). Most notable, the combination of MCC and CCS provided tablets with the most rapid disintegration.

Filler Type	Disintegrant Type	Thickness (mm)	Length (mm)	Width (mm)	Hardness (N)	Disintegration Time (sec)
MCC	CP	7.91±0.01	19.07±0.01	10.11±0.01	19.7±0.9	162.3±1.8
MCC	SSG	7.97±0.02	19.03±0.01	10.12±0.03	12.3±0.3	97.3±0.9
MCC	**CCS**	**8.08±0.01**	**18.97±0.02**	**10.09±0.01**	**8.0±0.6**	**54.7±1.8**
DCP	CP	7.81±0.01	19.04±0.01	10.10±0.01	19.3±1.2	152.7±4.3
DCP	SSG	7.87±0.07	18.98±0.03	10.06±0.01	14.3±0.9	115.7±11.0
DCP	CCS	8.05±0.04	19.03±0.01	10.13±0.03	10.0±0.6	90.3±1.2

Table 2. Tablet properties in study 3 using direct compression and dry granulation. Compaction force was varied.

	Compaction force (kN)	Mean compaction force (kN)	Mean compaction pressure (mPa)	In die porosity (%)	Heckel in die	Tensile strength (mPa)
Direct compaction	**1**	0.990±0.021	5.78±0.12	54.2±0.1	0.612±0.001	0.029±0.002
	2	2.01±0.01	11.7±0.1	49.2±0.1	0.700±0.001	0.109±0.009
	4	4.08±0.01	22.8±0.1	38.9±0.2	0.944±0.005	0.232±0.006
	7	7.02±0.01	41.0±0.1	27.5±0.5	1.29±0.02	0.743±0.062
	14	14.06±0.02	82.0±0.1	20.0±0.4	1.61±0.02	1.90±0.07
	17	17.05±0.02	99.5±0.1	17.1±0.5	1.77±0.03	2.41±0.03
Dry Granulation	**1**	0.953±0.009	5.56±0.05	49.9±0.1	0.696±0.001	0.029±0.002
	2	1.93±0.02	11.2±0.2	43.5±0.7	0.833±0.017	0.061±0.003
	4	3.83±0.05	22.3±0.3	36.0±0.4	1.02±0.01	0.123±0.006
	7	6.75±0.03	39.4±0.2	25.9±0.7	1.35±0.03	0.316±0.024
	14	13.96±0.07	81.5±0.4	18.7±0.4	1.68±0.02	0.757±0.018
	17	16.80±0.04	98.1±0.2	12.8±0.7	2.06±0.06	1.21±0.02

Table 3. Effects of tablet compaction force on RTN tablet properties for direct compression and dry granulation.

Compaction force (kN)	Hardness (N)	Thickness (mm)	% drug release at 60 min	$AUC_{0\text{-}60\ min}$ (µg.min/mL)
1kN	7.00±0.58	8.07±0.02	79.5±5.6	2020±320
2kN	23.7±0.9	7.61±0.01	96.9±0.5	2640±530
4kN	46.0±1.2	6.59±0.01	98.5±0.4	2710±550
7 kN	132±11	5.93±0.01	98.9±0.2	2710±540
14kN +4kN	22.3±1.2	6.08±0.03	97.0±0.1	2690±540
14kN +7kN	56.0±4.0	5.91±0.01	99.9±0.2	2750±550
14kN +14kN	151±2	5.36±0.02	27.2±0.1	666±119
14kN +17kN	191±3	5.29±0.01	20.4±0.4	481±80

Table 4. The observed and fitted permeation coefficient (P_{app}), k_p, flux (J_s) and the permeated amount of RTN solution and RTN tablets (Mean±SD, n=3)

	Permeation Coefficient (P_{app})(cm/sec) x10^6	Kp' (sec^{-1}) x10^6	Fitted Permeation Coefficient (P_{app})(cm/sec) x10^6	Kp' from fitted P_{app} (sec^{-1}) x10^6	Flux (Js) (µg min^{-1} cm^{-2})	Permeated amount % (at the end of 360 min)
Solution	9.30±1.83	1.19±0.2394	7.645±1.52*	0.977±0.195*	0.00100±0.00020	2.32±0.003
HPMCAS-L tablet	3.90±0.30	0.498±3.85	4.04±1.02**	0.517±0.106**	0.000430±0.000034	1.03±0.05

PVP-VA tablet	10.2±0.60	1.30±7.71	8.64±1.84**	1.10±0.92**	0.0618±0.0065	2.20±0.02
NORVIR tablet	14.7±8.46	1.88±1.09	8.72±4.60**	1.11±0.48**	0.00160+0.00090	2.02±0.64

* The equation of $M_b = M_0 - M_0 * e^{-kp't}$ (Figure 2) was used to fit the P_{app} values of solution from HFM. The fitted P_{app} was obtained via Solver.

**The fitted P_{app} for tablets were calculated via Eq.9 and Solver by using the k_d from tablet 'dissolution only' (0.398±0.0027 min^{-1} for HPMCAS-L; 0.0374±0.0010 min^{-1} for PVP-VA; 0.0239±0.0039 min^{-1} for Norvir Tablet) and kp' from the fitted P_{app} value (7.649 $x10^{-6}$ cm/sec) of solution from HFM. For conversion of k_p' and P_{app}, Eq.8 was used.